UNIVERSITÀ DELLA CALABRIA

UNIVERSITA' DELLA CALABRIA

Dipartimento di Ingegneria Informatica, Modellistica, Elettronica e Sistemistica

(DIMES)

Dottorato di Ricerca in

Information and Communication Technologies

CICLO

XXXII

ENHANCED ELECTROMAGNETIC MODELS FOR THE ACCURATE DESIGN OF NON-INVASIVE MICROWAVE BIOSENSORS

Settore Scientifico Disciplinare ING-INF/02

Coordinatore: Ch.mo Prof. Felice Crupi

Firma Firma oscurata in base alle linee guida del Garante della privacy

Supervisore/Tutor: Ch.mo Prof. Sandra Costanzo

Firma Firma oscurata in base alle linee guida del Garante della privacy

Dottorando: Dott. Vincenzo Cioffi

Firma [redacted]

Firma oscurata in base alle linee guida del Garante della privacy

Acknowledgements

To my supervisor Prof. Sandra Costanzo, for her continuous guidance, suggestions and patience during the course of my PhD. She puts a lot of effort into trying to make me a good researcher.

To Prof. Giuseppe Di Massa and the staff of Microwave Laboratory. I learned a lot from you-all.

To my girlfriend and my family for their constant support, motivation and love, which allowed me to carry out, in the best way, this research programme.

Vincenzo

TABLE OF CONTENTS

LIST OF FIGURES

1 INTRODUCTION

The general tendency of today's research is to make smart any aspect of our life, be it sports, or safety and even health.

In recent years, mobility is often equalized with wearability, where having all the devices and gadgets integrated in the clothes or mounted on the body offer the wearers' freedom in their daily activities. One of the last examples of wearable electronics are smart watches, which allow in their latest versions to perform analyses such as the ECG (Electrocardiogram) that were previously exclusive to hospitals or specialized centers. To undertake the classification and understanding of different wearable aspects, the Institute of Electrical and Electronics Engineers (IEEE), IEEE 802, established in December 2006 a task group, entitled IEEE 802.15.6, for the standardization of Wireless Body Area Network (WBAN) applications.

Depending on the type of communication, WBANs can be divided in three different categories: On-body, communication within the same body (wearer), Off-body, communication between the body (wearer) and an external unit, and In-body, communication between the implanted device in the body and device mounted on the body.

As mentioned before, these new wearable technologies are affecting different fields, including the medical one.

The main scope of this thesis is the development of a new non-invasive technology that can be a valid alternative to current devices for monitoring blood-glucose levels.

This issue is highly relevant, as diabetes mellitus is one of those diseases widespread especially in the so-called countries of well-being, where a sedentary lifestyle combined with high percentages of obesity promotes dissemination. ISTAT data for 2016 estimated at over 3 million, or 5.3% of the total population, the number of Italians suffering from this pathology. On

the level worldwide, on the other hand, the incidence rate of this pathology fluctuates between 5% and 8%.

Nowadays, glucose meters are a primary tool for the care of diabetic patients. At present, there isn't non-invasive monitoring technique of blood glucose concentration that is widely accepted in the medical industry.

The idea is to exploit the electromagnetic waves that penetrate biological tissues in a non-invasive way. The microwave fields when pass through the human body polarize the biological molecules and therefore the waves propagate more slowly than free space, then it is possible to design biosensors that convert these changes in the propagation speed into quantifiable signals that allow an estimate of biological parameters.

At the base of this idea there is a wearable biosensor which can therefore be easily integrated with daily clothing.

Although in the literature, several approaches of this type are already present, the most important novelties of this work are substantially two, the first is that of having developed an improved and more accurate version of the Cole-Cole dielectric model (useful for studying dielectric properties of blood at different glucose concentrations) and the second is to have realized the bio-sensor using fabrics, both for the substrate and for the conductive parts. Obviously, these two aspects will be explored later.

The proposed wearable antennas should be suitable for the integration into clothes allowing non-invasive and continuous monitoring, as current measuring instruments only allow invasive monitoring, in some cases even painful for the patient, but above all not continuous, in as limited to the single measurement related to the single blood sample.

The choice of materials, substrate and conductive, determines the mechanical characteristics of the wearable antennas in terms of their robustness and resilience against bending, twisting or being repellent to water.

In fact, the biggest challenge is to make the sensor as robust as possible to everyday life, so as to always obtain a precise and accurate measurement even in different situations and conditions. This bio-sensor, being integrated on the clothes will suffer bending, various wrinkling, without speaking of the different climatic conditions to which it will have to work.

1.1 Major Contributions of Present Work

The main contributions of present work can be collected in the three following aspects:

- An analytical model is elaborated starting from experimental data in order to better estimate the glucose concentration in the blood. In fact, the models present in the literature are incomplete or unreliable. Instead, this model permits the calculation of the dielectric constant and the tangent loss factor of the blood when change glucose concentration and operating frequency.
- A new approach to wearable antennas for a non-invasive continuous monitoring of blood glucose concentration is proposed. The novelty is the use of a textile substrate in order to realize sensors that can be integrated with everyday clothes. Fabrics have been used as dielectric substrate and, also, conductive textiles are commercially available and have been already used in textile antennas with excellent results.
- Some preliminary experimental tests have been conducted in order to validate the analytical model and therefore the realize biosensor.

2 TECHNOLOGIES FOR DIABETES MONITORING

Diabetes mellitus is a group of metabolic diseases in which a person has high blood sugar levels over a prolonged period. Symptoms of high blood sugar include frequent urination, increased thirst, and increased hunger.
Diabetes is due to either the pancreas not producing enough insulin, or the cells of the body not responding properly to the insulin produced. There are three main types of diabetes mellitus [1].

1. Type 1 diabetes, known as juvenile diabetes, is a condition in which pancreatic β-cell destruction usually leads to absolute insulin deficiency. This results in the inability to maintain glucose homoeostasis. Susceptibility to Type 1 diabetes is largely inherited, but there are also environmental triggers that are non-fully understood. About the 50-60 % of patients are under 18 years old.
2. Type 2 diabetes is characterized by a resistance to insulin, and in some cases absolute insulin deficiency. Lifestyles are significant factor in acquiring Type 2 diabetes. Type 2 diabetes includes 90% of people with diabetes around the world, and is largely the result of excess body weight and physical inactivity. Symptoms may be similar to those of Type 1 diabetes, but are often less marked. As a result, the disease may be diagnosed several years after onset, once complications have already arisen. Type 2 was seen only in adults but it is now also occurring in children.
3. Gestational diabetes is hyperglycaemia with onset or first recognition during pregnancy. Symptoms of gestational diabetes are similar to Type 2 diabetes. Gestational diabetes is most often diagnosed through prenatal screening, rather than reported symptoms. This type of diabetes is therefore a "physiological" phenomenon in some respects,

which as such does not normally involve serious dangers for the mother and the unborn child.

Since there is no cure for diabetes, it is controlled through the regulation of blood glucose levels. There are several types of measurements that can be used to monitor glucose regulation. Once in the blood stream, glucose combines with haemoglobin found in red blood cells (erythrocytes) to create glycated haemoglobin (HBA1C). The haemoglobin will remain glycated for the life of the erythrocyte, typically 90-120 days [2]. This makes HbA1c concentration measurement the best indication of average blood glucose concentration. While HbA1c measurements are the best method of long-term control, self-monitoring of blood glucose levels is fundamental to diabetes care. Frequent monitoring avoids hypoglycaemia, and aids in determining dietary choices, physical activity, and insulin doses.

Most at-home monitoring is performed with a blood glucose monitor. While current blood glucose monitors require small amounts of blood (2-10 μL) and can be used at sites other than the fingertips, it is still a painful and tedious measurement. Although blood glucose measurements fluctuate much more than HbA1c measurements, there is a strong correlation between HbA1c measurements and average glucose measurements taken over the same time period. Continuous monitoring systems also exist, but they require a subcutaneous injection to be replaced after a few days. While it has been shown that continuous monitoring systems are effective in reducing blood glucose to recommended levels, adolescents and young adults often have difficulty adhering to this intensive treatment. For this reason, non-invasive monitoring systems would be preferred.

Below some invasive, minimally invasive and non-invasive techniques will be discussed.

2.1 Invasive Glucose Monitoring Techniques

Currently, monitoring blood glucose concentration is most frequently measured through invasive techniques. The most common tool used is the glucose meter, Fig. 1. The measurement utilizes a lancing device on the side of a finger to produce a drop of blood. The drop of blood is placed on a test strip and the blood glucose meter calculates the blood glucose concentration and displays the results to the user. The blood sample is placed in contact with an enzyme (typically glucose oxidase) which produces hydrogen peroxide from glucose and oxygen. The hydrogen peroxide quantity is then measured amperometrically with a (typically platinum) electrode. The vast majority of monitoring systems sold today, whether continuous or blood meters, use enzyme-coated electrodes and amperometric analysis. Unfortunately, this method can be painful and painstaking to the user as the process needs to be repeated several times a day to ensure proper glucose concentration levels.

Figure 1 Some examples of glucose meters.

Moreover, for people who measure their blood glucose level several times a day, the measurement strips can become a significant expenditure. Clearly, a reusable, non-invasive glucose monitoring system would be beneficial. This has been a heavily researched field in recent years. Various non-invasive glucose monitoring techniques will be discussed in the next section.

2.2 Minimally Invasive Glucose Monitoring Techniques

In addition to purely invasive tools, such as standard glucometers there are also some different tools called minimally invasive sensors.

These are a first evolution of standard tools as they still require an invasive approach.

The minimally invasive sensors are based on different technologies: they measure blood sugar not directly in the blood, like invasive technologies, but in the interstitial fluid present in the subcutaneous tissue, starting from assumption that there is a direct relationship between subcutaneous glucose concentrations and plasma or capillary blood glucose. In this context, however, consider the so-called phenomenon defined as *alternative site testing (AST)* like phenomenon [3], or the possibility of a discrepancy in the measurement of glucose in alternative sites compared to capillary blood of the fingertip, to be attributed to the physiology of glucose distribution.

In fact, it has been found that in glycaemic stability conditions the glucose values in the alternative site accurately reflect the value of capillary blood sugar, while in the course of rapids glycaemic excursions, such as in the period postprandial, the interstitial fluid of the abdominal submucosal tissue varies with a certain difference in terms of both time and concentration. There is clear evidence showing how the alternative skin areas, such as the forearm or the abdomen wall, have a reduced capillary flow compared to fingertip. In addition, glucose sensors evaluate the concentration of glucose not in the bloodstream, but in interstitial fluids and is well documented as changes in glucose concentration in the blood and interstitial fluids do not occur simultaneously but with a certain delay, commonly referred to as lag time [4]. This, added to the sensor installation site, can explain the phenomenon AST. In particular, during rapid increases in blood sugar, interstitial glucose tends to rise more slowly (with a delay that has been quantified between 5

and the 20 minutes) and to reach lower hyperglycaemic peaks; on the contrary, during rapid reductions in blood glucose, the physiology of glucose interstitial is still controversial as it seems to times to follow over time, other times to precede the blood glucose variation. The confirmation of an advance in the reduction of glucose in the interstitial fluid was explained by the fact that hyperinsulinemia causes the entry of glucose into the cell starting right from the interstitial fluid, according to the scheme proposed in [5].

However, it has recently been highlighted, in a study conducted in the animal, which exists one close relationship between glucose concentrations a level of the subcutaneous tissue and those present in the brain tissue, where resides the glucose sensor which activates the counter-regulatory response to hypoglycaemia. Through intravenous injection of glucose and insulin in the experimental animal, it was actually verified that the sensor registered changes in the animal glucose concentration with a certain delay compared to what can be documented in the blood side, but that changes in glucose concentrations in the subcutaneous adipose tissue, in the muscle and in the cerebral cortex (where it is assumed to be present sensor for hypoglycaemia) appeared to occur in synchronous way, that is with the same delay compared to what can be documented in the blood [6].

2.3 Non-Invasive Glucose Monitoring Techniques

Opposed to invasive devices, non-invasive blood glucose monitors offer a solution to measure proper blood glucose levels without puncturing the skin. Non-invasive blood glucose monitoring has been tried with variety of different techniques. They have been divided into the following categories: interstitial fluid chemical analysis, breath chemical analysis, infrared spectroscopy, optical coherence tomography, temperature modulated localized reflectance, raman spectroscopy, polarity changes, ultrasound,

fluorescence, thermal spectroscopy, ocular spectroscopy, and impedance spectroscopy.

2.3.1 Interstitial Fluid Chemical Analysis

Interstitial Fluid (ISF) Chemical Analysis relies on an enzymatic reaction using the fluid excreted from the skin. A commercialized product was developed using interstitial fluid chemical analysis in the form of a watch. It was similar to traditional monitoring methods because it required the user to switch out disposable pads with each measurement [7].

2.3.2 Breath Chemical Analysis

This technique measures the level of acetone from a breath. Higher levels of acetone have been correlated to higher levels of blood glucose concentration. This method is however not as accurate as traditional blood glucose meters [8].

2.3.3 Infrared Spectroscopy

Infrared Spectroscopy can be separated into two categories: Near-infrared spectroscopy (NIR) and Mid-infrared spectroscopy (MIR).

NIR is a lower frequency measurement in which the transmission and reflection of infrared light is used to characterize blood glucose levels [9]. It is typically performed in an area of the body with relatively thin tissue like an earlobe. Due to the frequency of the light, this measurement is sensitive to changes in skin structure than can found in subjects with chronic hyperglycaemia.

MIR uses essentially the same technique as NIR, although there is typically not enough light penetration at MIR frequencies for transmission analysis to be performed. As a result, only reflection analysis is used [10].

2.3.4 Optical Coherence Tomography

Optical coherence tomography (OCT) is a specific form of light scattering measurement in which the phase component of reflected light is measured. OCT utilizes a low coherence (wide frequency spectrum) light source, which is sent from an interferometer to a reference mirror and to the subject (typically an arm) [11]. The reflected light from both the subject and the mirror are then correlated. By moving the subject location and the reference mirror location, an image can be generated with both lateral and in-depth scanning. An increase in ISF glucose levels causes an increase in refractive index, which can be seen in the generated images.

2.3.5 Temperature-modulated localized reference

This technique is another form of light scattering measurement. Biological tissues have varying refractive index based on temperature and on glucose concentration. By modulating skin temperature between 22 and 38 degrees C, variations in light packets reflected can be used to determine glucose levels [12].

2.3.6 Raman Spectroscopy

This is a method in which is generated an oscillation in a fluid which causes changes in light scattering properties. Specifically, this technique can be used to measure glucose concentrations in the front of the eye, in fact, is used a laser to stimulate glucose molecules to oscillate in the ocular fluid. The scattered light from the oscillation is an indicator of the glucose concentration. The disadvantage in this technique is the potential interference from other molecules [13].

2.3.7 Polarization Change

Polarization change is another optical technique being investigated in the eye. The polarization of a polarized light source will change angle slightly if it is passed through a solution of chiral molecules, such as glucose. While this technique is feasible, pH and interfering compounds have prevented high specificity [14].

2.3.8 Ultrasound

Several types of ultrasound techniques for monitoring glucose levels have been investigated, but they operate in the same principles. A short laser burst is used to locally heat a small tissue area, which causes an ultrasonic pulse to propagate through the tissue. The photoacoustic excitation is dependent on the laser frequency, as the laser frequency is varied, the concentration of glucose levels in fluids can be determined from the photoacoustic spectrum [15].

2.3.9 Fluorescence

A tissue excited using an ultraviolet laser generates a fluorescence at 380 nm. The intensity depends on glucose levels. The problem is that the intensity is strongly affected by skin pigment and thickness [9].

2.3.10 Thermal Spectroscopy

Thermal spectroscopy is the measurement of infrared radiation emitting from the human body. While other factors are significant as well, glucose concentration has been shown to have an absorptive effect on the quantity of human body infrared emission [7].

2.3.11 Ocular Spectroscopy

This is a method through which tears are chemically analyzed to reveal glucose levels, using a contact lens which reacts with the glucose in tears. When emitted with a light source, such as a laser, the reflected light changes wavelength based upon the glucose concentration, which can be measured with a spectrometer [16].

2.4 RF Transmission Technique

As mentioned usual devices are uncomfortable, due to their invasive nature, and they are not suitable for a continuous blood glucose monitoring. So, extensive research is being carried out in the last years for the development of non-invasive sensors able to overcome the aforementioned limitations, while maintaining the cost-effective and easy manufacturing features [17][18]. More recently, the adoption of microstrip technology has been proposed to realize low-cost microwave sensors to be placed near the human skin, with the aim to implement non-invasive blood glucose monitoring. Various different configurations can be found in literature, working in the reflection [19][20] or transmission mode, all based on the strict correlation between the blood permittivity and the blood glucose levels. Microwaves interact with materials and response size can be used for the determination of the composition of biological fluids and in the specific case the glucose concentration. There are three possible antenna glucose sensing models.
An overview is presented below:

1. **Implantable Active Sensing**

   In the implantable active sensing case, displayed in Fig. 2, the antenna acts as an active sensor. In this case, internal electronic circuitry and a power supply are needed for operation of the glucose sensing system.

This case could be ideal for a future implantable glucose sensor that also automatically dispenses insulin in real time.

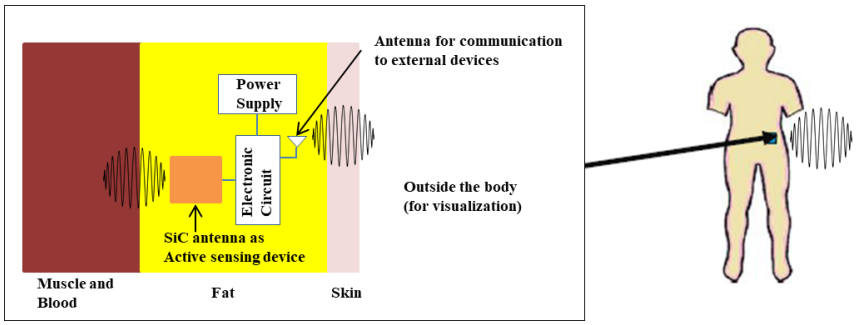

Figure 2 Active sensing antenna implanted in abdominal area configuration.

2. Implantable Passive Sensing

In the implantable passive sensing model, as displayed in Fig. 3, the antenna is implanted in fatty tissue and two additional external antennas (a transmitting and a receiving antenna) are required. The transmitting antenna sends a signal towards the implanted antenna, which is reflected to the receiving antenna by the implanted sensor and thus 'reads' the sensors resonance frequency. External circuitry records any glucose-induced changes in the implanted sensor's resonance frequency in addition to generating the required waveform.

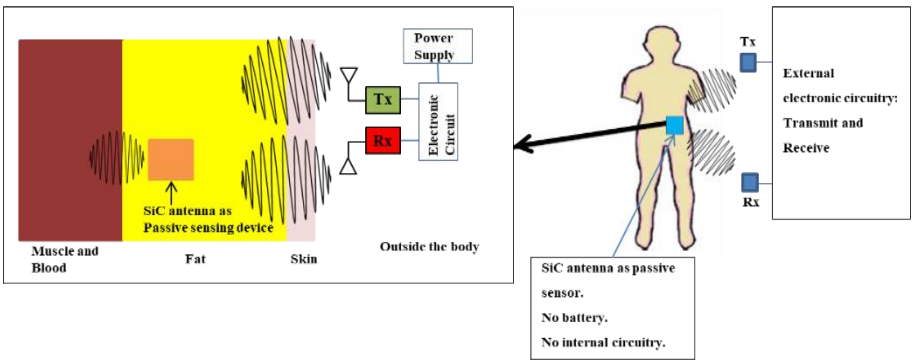

Figure 3 Implanted passive sensing antenna and external antennas configuration. The antenna implanted in the body does not require power supply or additional internal circuitry.

3. Non-Invasive Sensing

A non-invasive solution would be much more convenient for the patient, would not require surgery, and lower power Wi-Fi communication would be allowed due to no signal attenuation in human tissue. Fig. 4 displays an antenna patch located above the upper arm. The antenna and the external circuitry are located outside the body.

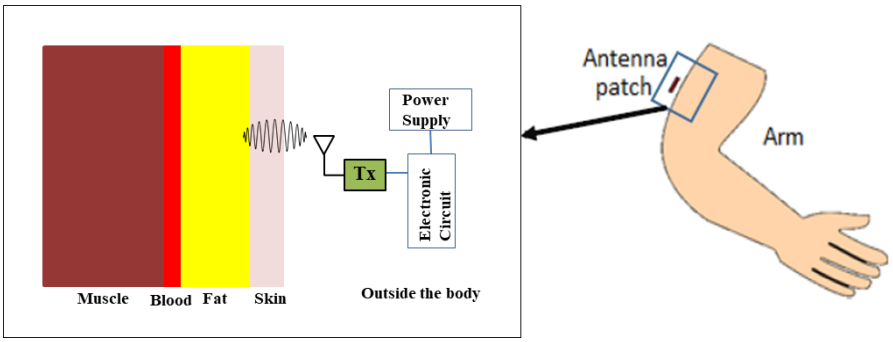

Figure 4 Non-invasive sensing antenna on top of the arm configuration. The antenna and the electronic circuitry are located outside the body.

3 GLUCOSE DEPENDENT PROPERTIES OF BLOOD

3.1 Dielectric Properties of Tissues

The most important effect arising from the interaction of an electric field with a dielectric material is **Polarization**. This phenomenon occurs when internal charge in the material moves in response to an external dielectric field, at the most fundamental level, electronic and atomic displacement take place in all dielectric materials. Molecules with permanent, induced or transient induced dipoles exhibit their own specific polarization. Biological materials contain free and bound charges including ions, polar molecules and an internal cellular structure [21]. The effect of an electric field is twofold: to trigger several polarization mechanisms, each governed by its own time constants, and to cause ionic drift. The result is the establishment of both displacement and conduction currents. For this reason, biological materials are classified as lossy dielectric materials.

At any time, the total polarization is the vector sum of all contributions such that:

$$P = \sum_i^n P_i \tag{1}$$

Irrespective of the molecular process, the polarization P is related to the dielectric displacement D, the internal dielectric field strength E and the dielectric properties as follows: $\underline{D}=\varepsilon_0\underline{E}$ in vacuum, and $\underline{D}=\varepsilon_0\varepsilon_r\underline{E}$ in a medium of permittivity ε_r relative to ε_0 which is that of free space. The latter expression may also be written as:

$$\underline{D} = \varepsilon_0\underline{E} + P \tag{2}$$

which describes the polarization P as a material-specific displacement vector. The dependence of *P* on *E* can take several forms, the simplest being a scalar proportionality such that:

$$P = \varepsilon_0(\varepsilon - 1)E \tag{3}$$

which defines the relative permittivity in terms of the polarization per unit field as:

$$\varepsilon = \frac{P}{\varepsilon_0 E} + 1 \tag{4}$$

The relative permittivity can be a tensor, a complex parameter or simply a real number depending on the directionality of the response and the phase difference between the displacement vector and the electric field. Assuming a linear, isotropic behaviour, the relative permittivity of biological materials is a complex parameter $\hat{\varepsilon}$ expressed as:

$$\hat{\varepsilon} = \varepsilon' - j\varepsilon'' \tag{5}$$

The real part ε' determines the component of the displacement current which is out-of-phase with the driving field, while the imaginary part ε" relates to the in-phase or power loss component and is referred to as loss factor. Considering displacement and ionic currents, a biological material is characterized by an effective conductivity σ and an effective loss factor ε" such that:

$$\varepsilon'' = \frac{\sigma}{\varepsilon_0 \omega} \tag{6}$$

and

$$\sigma = \sigma_d + \sigma_i \tag{7}$$

where the subscripts refer to displacement and ionic parameters. The conductivity σ is expressed in Siemens per meter *(S/m)* when ε_0 is expressed in *(F/m)* and ω in radians per second. The dielectric properties are usually presented as ε' and ε'' values, or ε' and σ values, as a function of frequency and, to a lesser extent, temperature.

3.1.1 Frequency Dependence of the Dielectric Properties of Tissues

The time dependence of the polarization is due to the various physical interactions and the time dependent response of the material to them. This is reflected in the frequency dependence of the permittivity. Three main interaction mechanisms, each governed by its own kinetics, determine the main features of the dielectric spectrum of a tissue. Three main spectral regions known as the α, β and γ dispersions are predicted from known interaction mechanisms.

The γ dispersion, in the gigahertz region, is due to the polarization of water molecules. The β dispersion, typically in the hundreds of kilohertz region, is due mainly to the polarization of cellular membranes that act as barriers to the flow of ions between the intra and extra cellular media. Other contributions to the β dispersion come from the polarization of protein and other organic macromolecules [21]. The low frequency α dispersion is associated with ionic diffusion processes at the site of the cellular membrane. In its simplest form, each dispersion is characterized by a single time constant τ and exhibits the following frequency dependence:

$$\hat{\varepsilon} = \varepsilon_\infty + \frac{\varepsilon_s - \varepsilon_\infty}{1 + j\omega t} \quad (8)$$

This is the well-known Debye expression, [22], in which ε_∞ is the permittivity at field frequencies where $\omega\tau >> 1$, and ε_s the permittivity at $\omega\tau << 1$. The magnitude of the dispersion is described as $\Delta\varepsilon = \varepsilon_s - \varepsilon_\infty$. The presence in a material of several mechanisms with relaxation times distributed around τ can be described in terms of a deviation from Debye behaviour and may be expressed as:

$$\hat{\varepsilon} = \varepsilon_\infty + \frac{\Delta\varepsilon}{1 + (j\omega t)^{(1-\alpha)}} \quad (9)$$

This is the semi-empirical Cole-Cole expression [23], in which the parameter α is introduced to describe the broadening of the dispersion. The spectrum of a tissue may be described mathematically in terms of multiple Cole-Cole dispersion and an ionic conductivity term such that:

$$\hat{\varepsilon} = \varepsilon_\infty + \sum_n \frac{\varepsilon_{sn} - \varepsilon_\infty}{1 + (j\omega t_n)^{(1-\alpha n)}} + \frac{\sigma}{j\omega\varepsilon_0} \quad (10)$$

where:

- ε_s is the low-frequency permittivity;
- ε_∞ is the high-frequency permittivity;
- τ gives the relaxation time;
- σ represents the ionic conductivity;
- ε_0 is the free-space permittivity;
- α is a parameter modelling the broadening of the dispersion lines.

The procedure to determine the parameters for several tissue types is reported in [24], and the parameters obtained are reported in Fig. 5.

Tissue type	ε_∞	$\Delta\varepsilon_1$	τ_1 (ps)	α_1	$\Delta\varepsilon_2$	τ_2 (ns)	α_2	$\Delta\varepsilon_3$	τ_3 (μs)	α_3	$\Delta\varepsilon_4$	τ_4 (ms)	α_4	σ
Blood	4.0	56.0	8.38	0.10	5200	132.63	0.10	0.0			0.0			0.7000
Bone (cancellous)	2.5	18.0	13.26	0.22	300	79.58	0.25	2.0×10^4	159.15	0.20	2.0×10^7	15.915	0.00	0.0700
Bone (cortical)	2.5	10.0	13.26	0.20	180	79.58	0.20	5.0×10^3	159.15	0.20	1.0×10^5	15.915	0.00	0.0200
Brain (grey matter)	4.0	45.0	7.96	0.10	400	15.92	0.15	2.0×10^5	106.10	0.22	4.5×10^7	5.305	0.00	0.0200
Brain (white matter)	4.0	32.0	7.96	0.10	100	7.96	0.10	4.0×10^4	53.05	0.30	3.5×10^7	7.958	0.02	0.0200
Fat (infiltrated)	2.5	9.0	7.96	0.20	35	15.92	0.10	3.3×10^4	159.15	0.05	1.0×10^7	15.915	0.01	0.0350
Fat (not infiltrated)	2.5	3.0	7.96	0.20	15	15.92	0.10	3.3×10^4	159.15	0.05	1.0×10^7	7.958	0.01	0.0100
Heart	4.0	50.0	7.96	0.10	1200	159.15	0.05	4.5×10^5	72.34	0.22	2.5×10^7	4.547	0.00	0.0500
Kidney	4.0	47.0	7.96	0.10	3500	198.94	0.22	2.5×10^5	79.58	0.22	3.0×10^7	4.547	0.00	0.0500
Lens cortex	4.0	42.0	7.96	0.10	1500	79.58	0.10	2.0×10^5	159.15	0.10	4.0×10^7	15.915	0.00	0.3000
Liver	4.0	39.0	8.84	0.10	6000	530.52	0.20	5.0×10^4	22.74	0.20	3.0×10^7	15.915	0.05	0.0200
Lung (inflated)	2.5	18.0	7.96	0.10	500	63.66	0.10	2.5×10^5	159.15	0.20	4.0×10^7	7.958	0.00	0.0300
Muscle	4.0	50.0	7.23	0.10	7000	353.68	0.10	1.2×10^6	318.31	0.10	2.5×10^7	2.274	0.00	0.2000
Skin (dry)	4.0	32.0	7.23	0.00	1100	32.48	0.20	0.0			0.0			0.0002
Skin (wet)	4.0	39.0	7.96	0.10	280	79.58	0.00	3.0×10^4	1.59	0.16	3.0×10^4	1.592	0.20	0.0004
Spleen	4.0	48.0	7.96	0.10	2500	63.66	0.15	2.0×10^5	265.26	0.25	5.0×10^7	6.366	0.00	0.0300
Tendon	4.0	42.0	12.24	0.10	60	6.37	0.10	6.0×10^4	318.31	0.22	2.0×10^7	1.326	0.00	0.2500

Figure 5 Parameters of equation (10) used to predict the dielectric properties of different tissues, [24].

3.2 Limitations of the Standard Cole-Cole Model

Actually, the Cole-Cole model represents the most efficient dielectric representation of biological tissues response over frequency.

The aim of this thesis is to implement a new non-invasive technology for monitoring blood glucose levels.

One of the difficulties in designing sensors for monitoring blood glucose levels is that blood samples with different BGC are difficult to find as well as difficult to treat as they also require precise preservation procedures in order to avoid the deterioration of the sample and therefore the modification of its chemical and dielectric characteristics.

For this reason, it is evident that the standard Cole-Cole model (Eq. 10) presents a problem, in fact, when applied to blood plasma, the above dielectric models reveal a strong limitation, as no correlation exists between the complex permittivity and the blood glucose concentration, thus resulting into inaccurate design of microwave biomedical devices. If used the multiple dispersion form, with two poles, (n=2), it is possible to calculate the dielectric constant and the tangent loss factor when changes the frequency, but it is not possible consider the blood glucose concentration.

To solve this limitation in the literature are present different solutions.
In the next paragraph, two possible and partial solutions to the problem will be analysed.
Then, a new improved version of the standard Cole-Cole model will be presented and discussed, developed specifically for this project.

3.2.1 Different Approaches of Dielectric Model Present in the Literature

The first modified version of the Cole-Cole model is reported in [25]. In this study, has been shown a correlation between electrical properties (relative permittivity and conductivity) of blood plasma and glucose concentration, has been assumed that the changes in other minerals in the blood plasma such as calcium, chloride, potassium, and magnesium will have very minor or no effects on the electrical properties. For instance, the glucose concentration in a diabetic patient's blood may vary between 30 mg/dl and 400 mg/dl while sodium and chloride levels, although they exist in large quantities, only vary from 310 mg/dl to 333 mg/dl and 337 mg/dl to 372 mg/dl, respectively. For this work, have been performed electrical property measurements on blood samples collected from 10 adults between the ages of 18 and 40, and the measurements are conducted between 500 MHz and 20 GHz band. Each sample is then measured at eight different glucose concentrations: 0 mg/dl, 250 mg/dl, 500 mg/dl,1000 mg/dl, 2000 mg/dl, 4000 mg/dl, 8000 mg/dl and 16000 mg/dl. Measurements are repeated three times for each sample to ensure data reliability.
Following the measurements, the wideband dielectric properties at each glucose concentration are fitted to the single pole Cole-Cole model, (Eq. 10).

All calculations are carried out using particle swarm optimization, **PSO** that is an iterative technique that models the solution process after the natural movement of groups such as swarms of bees.

In the formula, to limit the number of parameters, the pole broadening parameter, $\boldsymbol{\alpha_n}$, is fixed at 0.1, because this parameter doesn't change significantly among various body tissues and has an average value of 0.1. The calculated parameters, in this work, for each glucose concentration are reported in Table 1:

Table 1: Parameters for single pole Cole-Cole model.

	0 [mg/dl]	**250 [mg/dl]**	**500 [mg/dl]**	**1000 [mg/dl]**	**2000 [mg/dl]**	**4000 [mg/dl]**	**8000 [mg/dl]**	**16000 [mg/dl]**
$\boldsymbol{\varepsilon_\infty}$	2.8	2.04	2.67	2	2.11	3.1	3.29	5.63
$\boldsymbol{\Delta\varepsilon}$	70.02	70.72	70.41	70.85	70.81	69.08	68.37	64.87
τ [ps]	8.68	8.62	8.88	8.86	9.32	9.51	10.57	12.6
$\boldsymbol{\sigma_i}$ **[S/m]**	2.13	1.96	1.93	1.73	1.46	1.66	1.31	1.38

The dielectric constant and the tangent loss factor behaviour obtained using this model is shown in Fig. 6 and in Fig. 7.

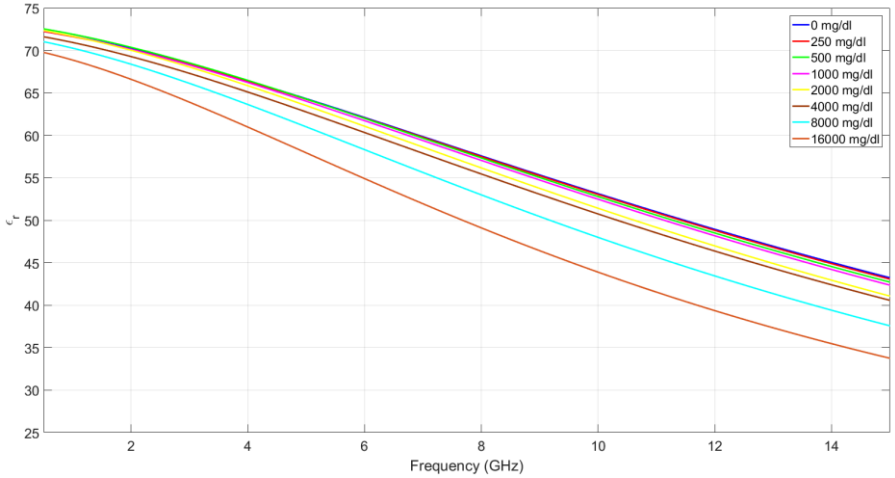

Figure 6 Dielectric constant behaviour obtained with [21].

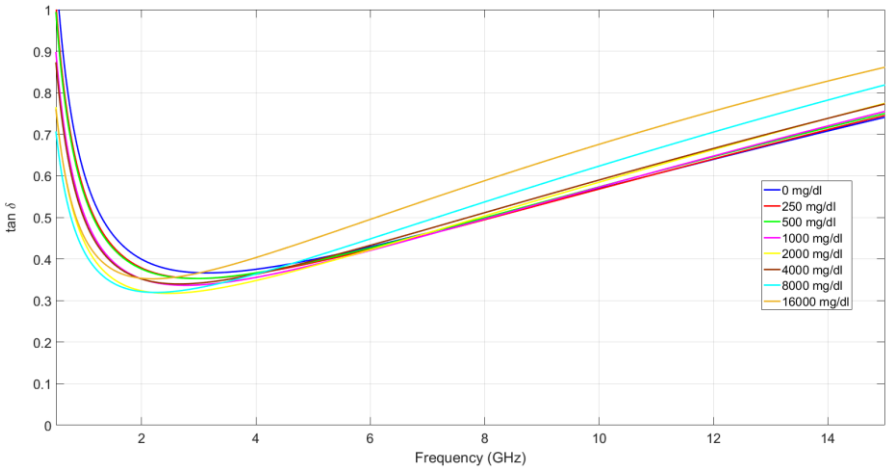

Figure 7 Tangent loss factor behaviour obtained with [21].

In this case, it is evident a variation of the dielectric properties when changes the operating frequency and the BGC. In the Table 2, are reported the values extrapolated from the curves at 2.4 GHz (ISM-Band).

Table 2: Dielectric constant and tangent loss factor values @2.4 GHz.

[mg/dl]	**ε_r**	**tanδ**
0	69.51	0.3778
250	69.45	0.3605
500	69.66	0.3592
1000	69.41	0.3395
2000	69.26	0.3174
4000	68.51	0.3413
8000	67.51	0.3201
16000	65.55	0.3533

At this frequency, there is a very small variation of the values, this could be a problem in the bio-sensor design. In fact, the sensor may not be able to distinguish the various concentrations, especially in the range 0-300 mg/dl which is the one required to be evaluated.

This work includes also some functions to fit the calculated Cole-Cole parameters in order to minimize the differences between measurements and calculated values.

In the literature, is present another modified version of the standard Cole-Cole model that includes the glucose level in its formula [26].

In that work, has been performed an in-vitro study in which 20 subjects volunteered (8 diabetics and 12 non diabetics) to have two samples of their blood drawn. Two samples of 3 ml were taken, one in a vial containing Ethylenediaminetetraacetic acid (EDTA) and one without any additives. EDTA is a chelating agent, which sequesters the iron molecules in the blood to prevent clotting. The blood with EDTA was tested in the laboratory for glucose concentration. The blood without additives was placed in a 5 ml dish and the dielectric properties were measured with an Agilent 8720B Network Analyzer and an Agilent 85070E dielectric probe. The in-vitro measurements of dielectric permittivity and conductivity have been conducted, and a correction factor for the standard Cole-Cole model has been elaborated. This correction factor has been obtained by curve fitting to include glucose level $\boldsymbol{g}$, in the real part as given in (11):

$$\hat{\varepsilon} = Re[\varepsilon_\infty + \sum_n^2 \frac{\Delta\varepsilon_n}{1+(j\omega t_n)^{(1-\alpha_n)}}] \cdot [(-0.001445)\boldsymbol{g} + \\ +1.145882] + Im\left[\varepsilon_\infty + \sum_n^2 \frac{\Delta\varepsilon_n}{1+(j\omega t_n)^{(1-\alpha_n)}} + \frac{\sigma_i}{j\omega\varepsilon_0}\right]. \quad (11)$$

The parameters used in (11) are reported in Table 3.

Table 3: Parameters used for double poles (n=2) Cole-Cole formula.

$\boldsymbol{\varepsilon_\infty}$	$\boldsymbol{\Delta\varepsilon_1}$	$\boldsymbol{\Delta\varepsilon_2}$	$\boldsymbol{\tau_1}$ **[ps]**	$\boldsymbol{\tau_2}$ **[ps]**	$\boldsymbol{\alpha_1}$	$\boldsymbol{\alpha_2}$	$\boldsymbol{\sigma_i}$
2.8	56.5	5500	8.377	132.629	0.057	0.1	0.5

The parameter $\boldsymbol{g}$, indicates precisely the concentration expressed in mg/dl. Obviously, the limit of this model is that the BGC influences only the real part, leaving the imaginary part constant as the glucose concentration variation. This is a limit in the calculation of the tangent loss factor, which is

given by the relationship between the imaginary part and the real part of the complex permittivity.

Using this model, have been calculated the behaviours of the dielectric constant, Fig. 8, and the tangent loss factor, Fig. 9.

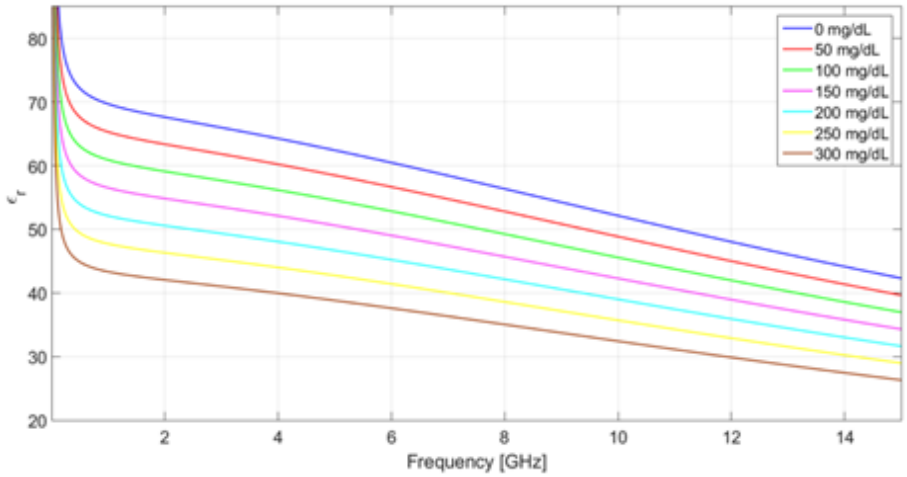

Figure 8 Dielectric constant behaviour.

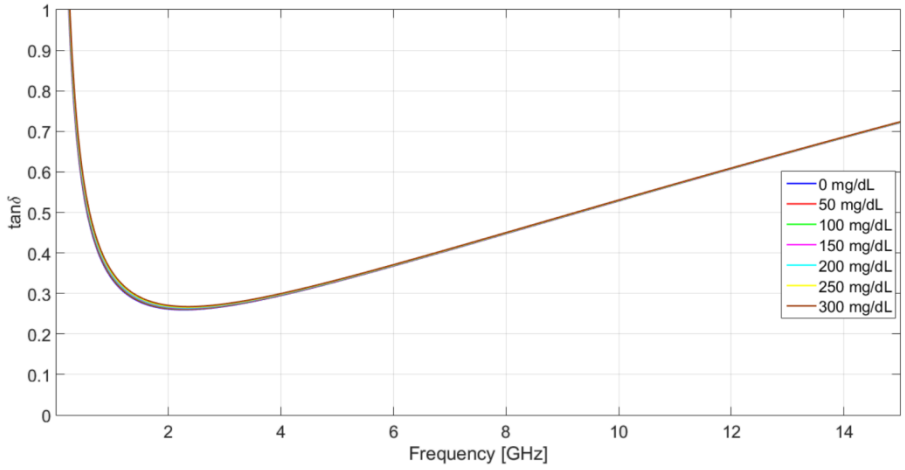

Figure 9 Tangent loss factor behaviour.

In Fig. 9, it would seem a constant tangent loss factor when the BGC changes, in reality, a slight variation is present.

This variation can be appreciated thanks to the zoom of Fig. 9 shown in Fig. 10.

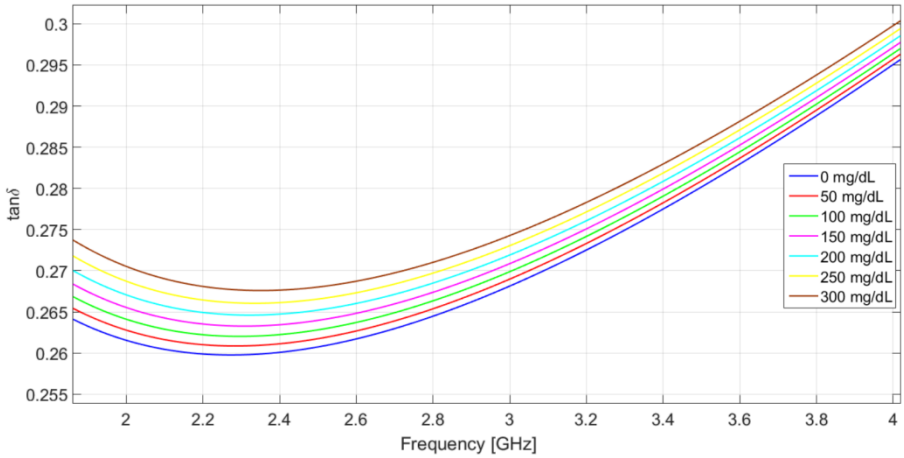

Figure 10 Zoom of the tangent loss factor behaviour.

The tangent loss factor is the relationship between the imaginary part and the real part of the complex dielectric permittivity:

$$tan\delta = \frac{-Im(\varepsilon)}{Re(\varepsilon)} \tag{12}$$

The problem, with this modified model, is that only the real part of the permittivity varies with the variation of BGC.

In the Table 4, are reported the values extrapolated at 2.4 GHz. These values are different but very similar.

Table 4: Values extrapolated from the curves in the Figure 9 and Figure 10.

[mg/dl]	**ε_r**	**tanδ**
0	66.97	0.2601
50	62.75	0.2611
100	58.53	0.2622
150	54.31	0.2634
200	50.08	0.2647
250	45.86	0.2661
300	41.64	0.2676

4 ENHANCED COLE-COLE DIELECTRIC MODEL FOR ACCURATE BLOOD GLUCOSE SENSING

In order to solve the problems and limitations of the dielectric models seen, an improved and corrected version of the two poles Cole-Cole model is proposed, which extends the Eq. (10), introducing a correction factor also for the imaginary part of the complex permittivity.

The importance of the variation of the loss tangent factor for a correct sensor design has already been treated in the literature, and has been shown that the loss tangent factor variation of the blood medium should be properly taken into account, in order to achieve reliable results, [27] [28].

For this reason, an enhanced dielectric model, basically adopting the two-poles Cole-Cole model, is proposed, which extends the modified Eq. (11) by including also a correlation between the imaginary part of the blood permittivity and the glucose concentration. Considering that complex permittivity curves of water-glucose and blood-glucose solutions show similar functional behaviour (both in terms of real as well as imaginary part), [29], this improved model is obtained by performing an accurate fitting on the measured data captured with an open-ended coaxial probe, on water solutions with different glucose concentrations.

Human blood is a tissue made up of a liquid part, plasma and figurative elements consisting of red blood cells, white blood cells and platelets. Plasma is a 55% yellow liquid in the blood. It is made up of 90% water, where organic substances (9%) and inorganic substances (1%) are dissolved. Plasma proteins are present in the organic part: albumins, globulins and fibrinogen.

Considering the dielectric trends observed above, is expected that the dielectric constant decreases and the tangent loss factor increases as the glucose concentration and the frequency increases.

4.1 Measurements on Water-Glucose Solutions

Before carrying out the measurements, conducted at the µWave laboratory in the University of Calabria, the water-glucose solutions have been prepared.
The choice of concentrations to be used has been made considering the typical blood glucose values of a healthy human subject and a person suffering from diabetes, so as to have a feedback as realistic as possible. In the Table 5, are reported the typical glycaemia levels.

Table 5: Clinical Glycaemia Levels.

Target levels (by type)	Upon waking	Before meals	At least 90 minutes after meals
Non-diabetic		72 to 106 mg/dl	under 140 mg/dl
Type 2 diabetes		72 to 126 mg/dl	under 153 mg/dl
Type 1 diabetes	90 to 126 mg/dl	72 to 126 mg/dl	90 to 162 mg/dl
Children w/ type 1 diabetes	72 to 126 mg/dl	72 to 126 mg/dl	90 to 162 mg/dl

In order to have wider concentration ranges, have been chosen glucose levels ranging from 100 mg/dl to 500 mg/dl.
Using the technique of "Coaxial probe", the permittivity values of the mixtures prepared have been measured.
As said, has been used the *"Open Ended-Coaxial Probe Technique"*, where the coaxial probe, Fig. 11, has been connected to the Vector Network Analyzer (VNA).

Figure 11 Open-Ended Coaxial Probe (Courtesy of https://speag.swiss/).

The coaxial probe used, built by SPEAG, measures the ε_r in a range from 1 to 200. It introduces a measurement uncertainty equal to ±2%, as reported in Calibration Certificate provided by Calibration Laboratory of SPEAG.
The fields radiated by the probe interact with the material put in contact with its interface. The reflection at the inlet of the probe varies in relation to the variation of dielectric permittivity of the material in contact.
The medium under test, in the specific case the water-glucose mixtures, must appear as semi-infinite, so it must have a greater extension than the diameter of the sensor opening. Furthermore, there must be no air gap between the sensor and the sample.
The measurements setup prepared in the laboratory is reported in the Fig. 12.

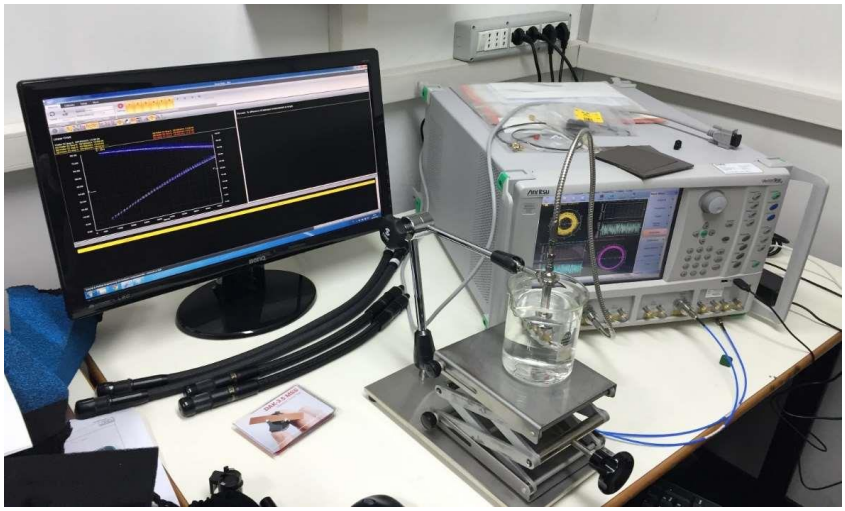

Figure 12 Measurements setup in the µWave Laboratory at the University of the Calabria.

The measurements have been performed using a VNA by Anritsu and the solutions have been put into the becher.
The first measurement has been conducted on a pure water sample at 22°C, in the next figure is shown the behaviour measured.

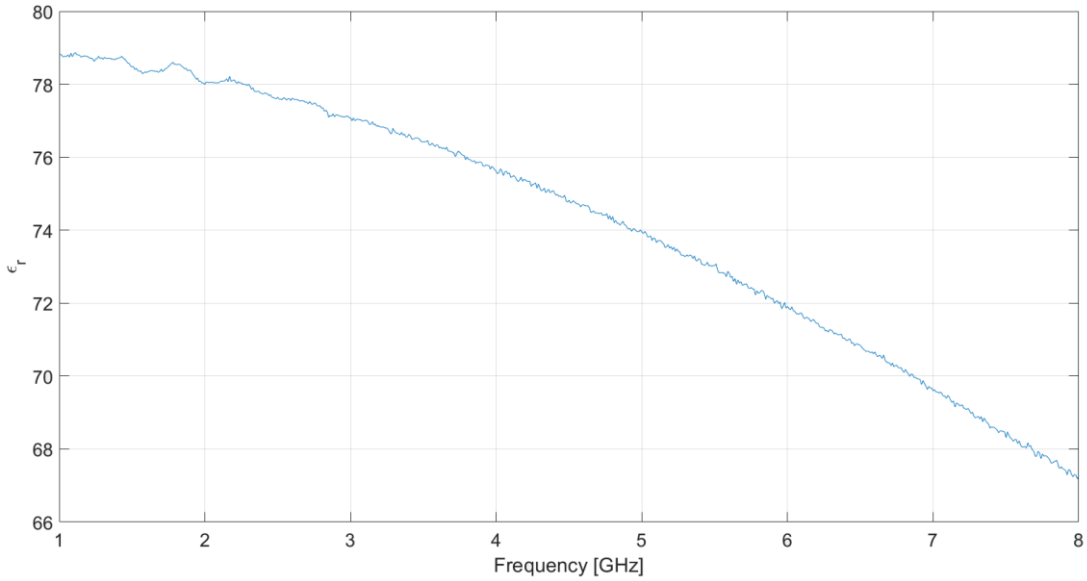

Figure 13 Dielectric constant real part behaviour measured on pure water at 22°C.

The trend of the ε_r real part, as expected, is decreasing as the frequency increases.

After this preliminary measurement, has been measured the complex permittivity of the various mixtures prepared. Every measurement is repeated five times for each solution to ensure data reliability. In the next figures, the average of these measurements is reported.

The Fig. 14 and 15 report respectively the measured trends of the real part of the permittivity and the tangent loss factor.

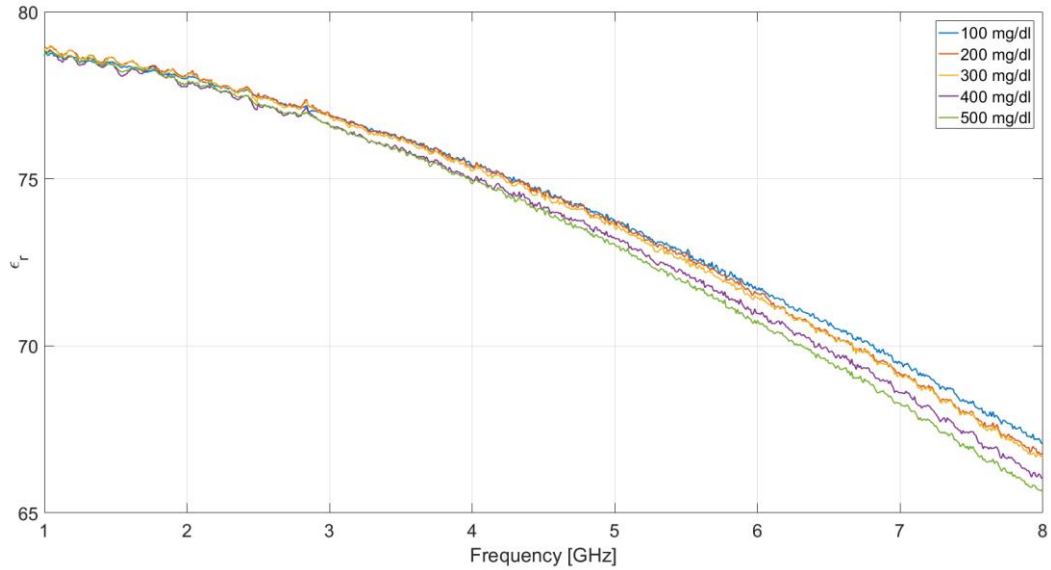

Figure 14 Dielectric constant real part behaviour for different water-glucose solutions.

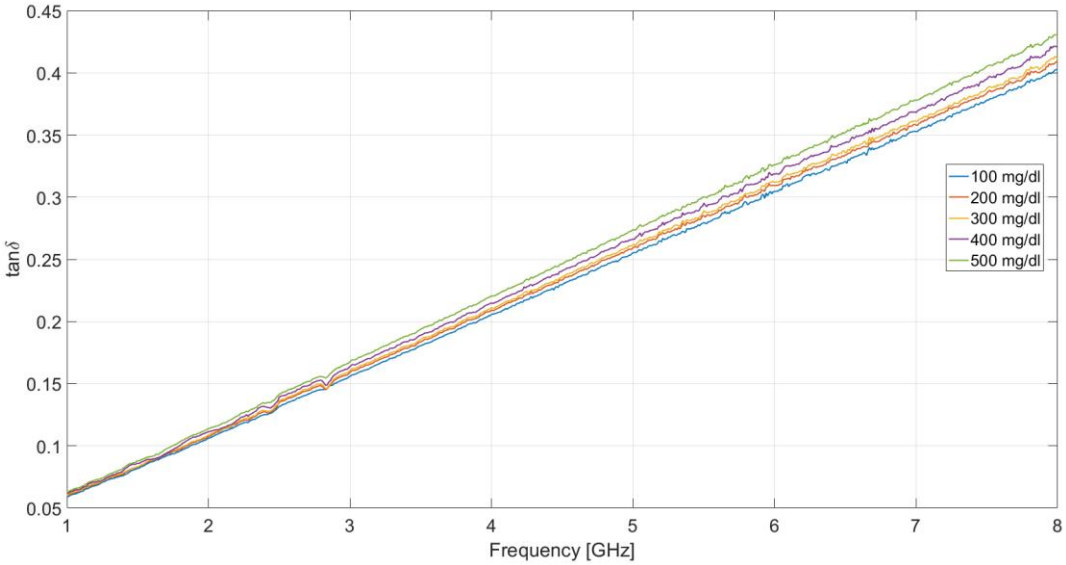

Figure 15 Tangent loss factor behaviour for different water-glucose solutions.

The measurements are in accordance with expectations, in fact, the real part of ε_r decreases with increasing frequency and glucose concentration, while the tangent loss factor increases with increasing glucose concentration and frequency.

4.2 Step by Step Procedure for the Elaboration of the Correction Factor for the Imaginary Part of the Dielectric Model

Using these measurements has been possible through a curve fitting performed on Matlab to be able to elaborate a correction factor for the imaginary part of the complex permittivity. The procedure is descripted below.

The dielectric model part to be modified is the following:

$$Im(\hat{\varepsilon}) = \varepsilon_{\infty} + \sum_{m=1}^{2} \frac{\Delta\varepsilon_m}{1+(j\omega\tau_m)^{(1-\alpha_m)}} + \frac{\sigma_i}{j\omega\varepsilon_0}. \qquad (13)$$

In order to formulate a correction factor by including also a correlation between the imaginary part of the blood permittivity with the glucose concentration and the operating frequency, the first step is to choose a reference frequency, in the first case equal to 2.4 GHz. The values corresponding to 2.4 GHz of the imaginary part of the dielectric permittivity have been extrapolated from the measurements on water-glucose solutions, and are reported in the Table 6.

Table 6: Imaginary part of the complex permittivity at 2.4 GHz.

mg/dl	**Im(ε)**
100	9.7074
200	9.8962
300	9.9265
400	10.1887
500	10.3713

Also for the standard Cole-Cole model has been extrapolated the imaginary part of the complex permittivity ad 2.4 GHz, obviously, this value is a constant, since it doesn't depend on the BGC (Blood Glucose Concentration). This value is 17.21.

It has been necessary to relate the data measured to the different concentrations with the data extrapolated from the curve resulting from the standard model.

The relationship between the measured data and the data calculated by the model has been therefore made, in order to have a correlation between the available data, all dependent on the BGC. Using these new data and the Curve Fitting Tool on Matlab, the approximation curve has been calculated and the polynomial function obtained is the following:

$$FC(BGC) = (9.4 \cdot 10^{-5} \cdot BGC) + 0.5539. \quad (14)$$

This result has been added in (13), and the result is:

$$Im(\hat{\varepsilon}) = [\varepsilon_{\infty} + \sum_{m=1}^{2} \frac{\Delta\varepsilon_m}{1+(j\omega\tau_m)^{(1-\alpha_m)}} + \frac{\sigma_i}{j\omega\varepsilon_0}] \cdot (9.4 \cdot 10^{-5} \cdot BGC + 0.5539). \quad (15)$$

The following figure shows the imaginary part behaviour as the glucose concentration varies:

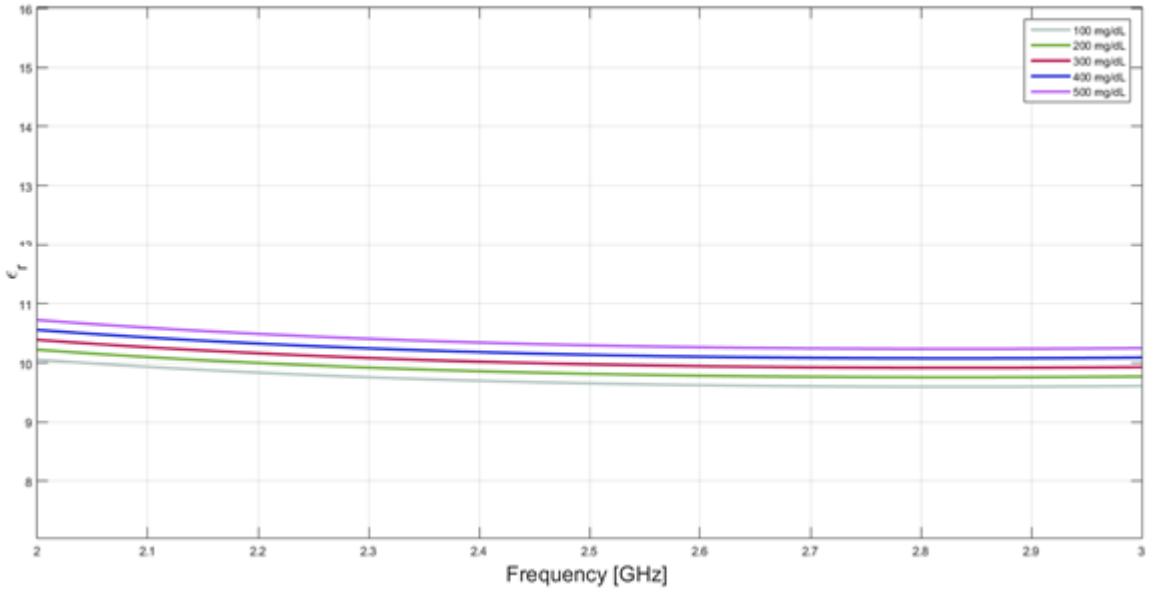

Figure 16 Tangent loss factor behaviour for different water-glucose solutions.

The trend shown is coherent with what is shown by the measurements, a growing trend with increasing concentration. The same procedure has been performed at 5 GHz and 7 GHz.

The polynomial functions obtained are:

- For 5 GHz:

$$FC(BGC) = (0.0001428 \cdot \mathrm{BGC}) + 0.9775. \quad (16)$$

- For 7 GHz:

$$FC(BGC) = (0.0001427 \cdot \mathrm{BGC}) + 1.123. \quad (17)$$

Using the previous functions, the correction factors for the individual concentrations have been calculated for a single frequency, the values obtained are shown in the Table 7:

Table 7: Correction Factors at Single Frequency.

Frequency [GHz]	**100 mg/dl**	**200 mg/dl**	**300 mg/dl**	**400 mg/dl**	**500 mg/dl**
2.4	0.5637	0.5727	0.5821	0.5915	0.6009
5	0.9918	1.0061	1.0203	1.0346	1.0489
7	1.1373	1.1515	1.1658	1.1801	1.1944

Starting from these values a new curve fitting has been performed, placing the three frequencies on the x-axis and the correction factors of the individual concentrations (Table 7) on the y-axis, thus obtaining five new approximation functions dependent on frequency expressed in Hz.

The correction factors obtained after this second curve fitting are shown below:

- For 100 mg/dl:

$$G(f[Hz]) = (0.1267 \cdot f) + 0.2891 \quad (18)$$

- For 200 mg/dl:

$$G(f[Hz]) = (0.1278 \cdot f) + 0.2965 \quad (19)$$

- For 300 mg/dl:

$$G(f[Hz]) = (0.1289 \cdot f) + 0.3039 \quad (20)$$

- For 400 mg/dl:

$$G(f[Hz]) = (0.13 \cdot f) + 0.3112 \quad (21)$$

- For 500 mg/dl:

$$G(f[Hz]) = (0.1311 \cdot f) + 0.3186 \quad (22)$$

Thus, five approximation functions depending on f[Hz] have been obtained, these functions have the following form:

$$G(x) = a \cdot x + b \tag{23}$$

Both coefficients **a** and **b**, with varying concentration, have a constant increase when the glucose concentration varies.

Therefore, has been possible to develop a single correction factor dependent on the BGC and on the operating frequency:

$$\boldsymbol{FC} = [\mathbf{0.1256} + (\mathbf{0.000011} \cdot \boldsymbol{BGC})] \cdot \frac{\boldsymbol{\omega}}{\mathbf{2\pi}} + [\mathbf{0.2817} + \\ +(\mathbf{0.000074} \cdot \boldsymbol{BGC})]. \tag{24}$$

The imaginary part of the dielectric model becomes:

$$Im(\hat{\varepsilon}) = [\varepsilon_\infty + \sum_{m=1}^{2} \frac{\Delta\varepsilon_m}{1+(j\omega\tau_m)^{(1-\alpha_m)}} + \frac{\sigma_i}{j\omega\varepsilon_0}] \cdot FC. \tag{25}$$

Simulating only the imaginary part of the complex permittivity with the correction factor processed the result is shown in the Fig. 17.

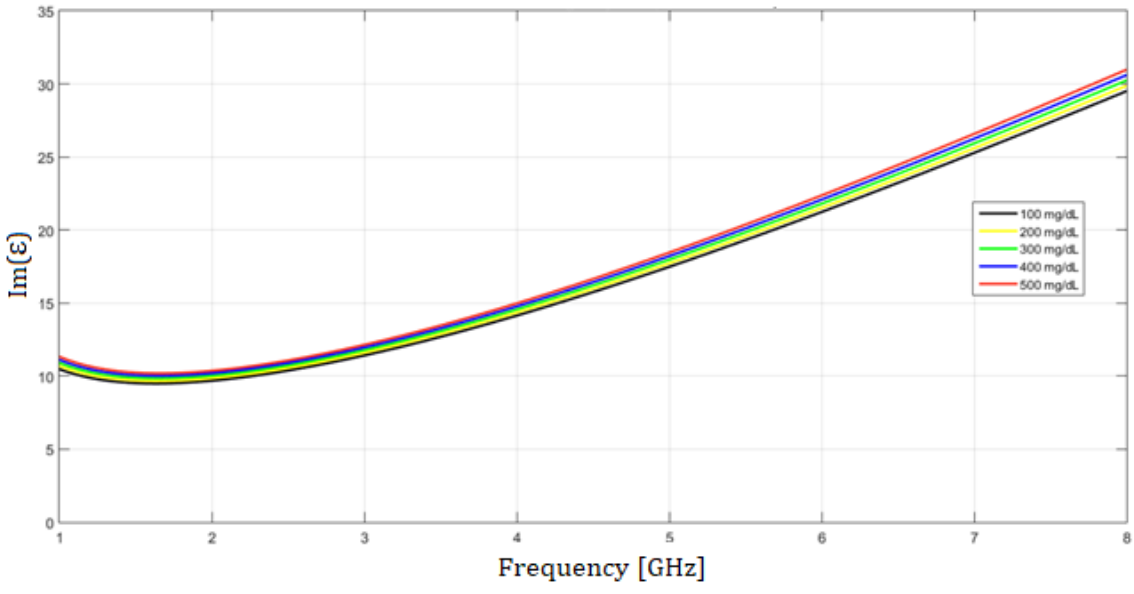

Figure 17 Corrected imaginary part of dielectric model.

It's evident that with the new correction factor there is a trend of the imaginary part in agreement with what has been described previously.
Therefore, the enhanced version of the Cole-Cole model for accurate blood glucose sensing is the following:

$$\hat{\varepsilon} = Re\left[\varepsilon_\infty + \sum_n^2 \frac{\Delta\varepsilon_n}{1+(j\omega t_n)^{(1-\alpha_n)}}\right] \cdot [(-0.001445)g + 1.145882] + Im\left[\varepsilon_\infty + \sum_n^2 \frac{\Delta\varepsilon_n}{1+(j\omega t_n)^{(1-\alpha_n)}} + \frac{\sigma_i}{j\omega\varepsilon_0}\right] \cdot [0.1256 + (0.000011 \cdot BGC)] \cdot \frac{\omega}{2\pi} + +[0.2817 + (0.000074 \cdot BGC)]. \quad (26)$$

This enhanced dielectric model has been presented in [30].

4.3 First Preliminary Numerical Validations

In the present section, the accuracy improvement introduced by the proposed model (26) is numerically validated on the microwave sensor configuration first reported in [27][31], and illustrated in Fig. 18. It is a standard inset-fed patch antenna working in the Industrial, Scientific, Medical (ISM) band around a frequency f_0 = 2.4 GHz, and printed on a dielectric substrate with high permittivity (ε_r = 10) to reduce as much as possible the effect of environmental properties. Experimental validations of the microwave sensor on water-glucose solutions have been successfully discussed in [27][31], where the importance of assuming the loss tangent variations versus the glucose level is also highlighted with the aim to improve the microwave antenna sensitivity.

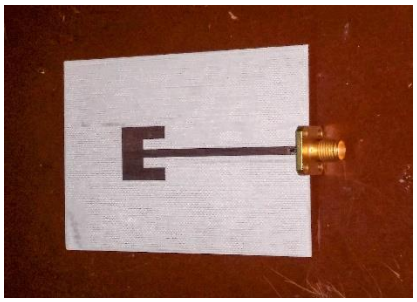

Figure 18 Microwave sensor discussed in [23][26].

4.3.1 Biological Stratified Medium Considered as Superstrate

The location for the bio-sensor is on the upper human arm, as displayed in Fig. 19.

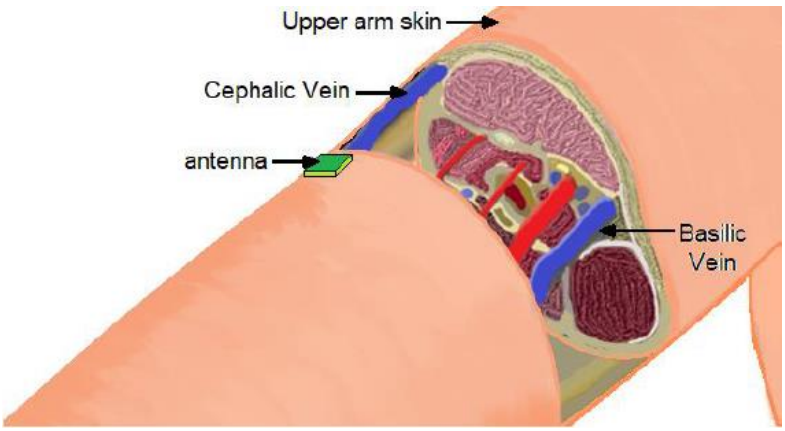

Figure 19 Bio-sensor location over the arm showing cross sectional anatomy.

For this reason, the microwave sensor is numerically validated by assuming a simplified model of the human arm well simulating the biological stratified tissues, and detailed in Fig. 20.

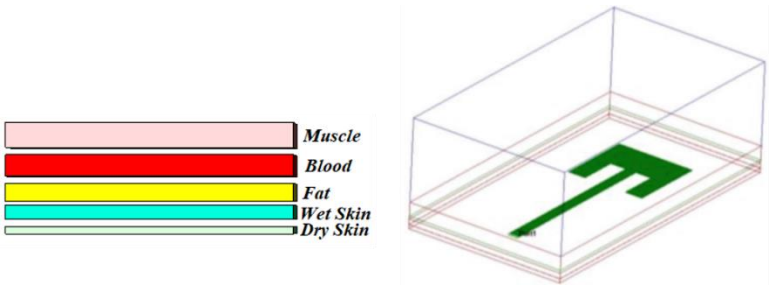

Figure 20 Stratified configuration for simulations of microwave sensor in Fig. 20.

This superstrate is a simplified model of a human arm. The dielectric characteristics considered are reported in Table 8.

Table 8: Dielectric characteristics of stratified biological superstrate.

Medium	**Thickness [mm]**	**ε_r**	**tanδ**
Dry Skin	0.015	38.06	0.2835
Wet Skin	0.985	42.92	0.2727
Fat	1.5	10.84	0.1808
Blood	2.5	/	/
Muscle	15.2	52.34	0.1893

The standard Cole-Cole model [23] is adopted to obtain the dielectric parameters for the media in the superstrate, while for the blood layer have been used the three dielectric model discussed before, [25][26][30].

The following figures show the dielectric constant behaviour of the layers considered obtained with the standard Cole-Cole model.

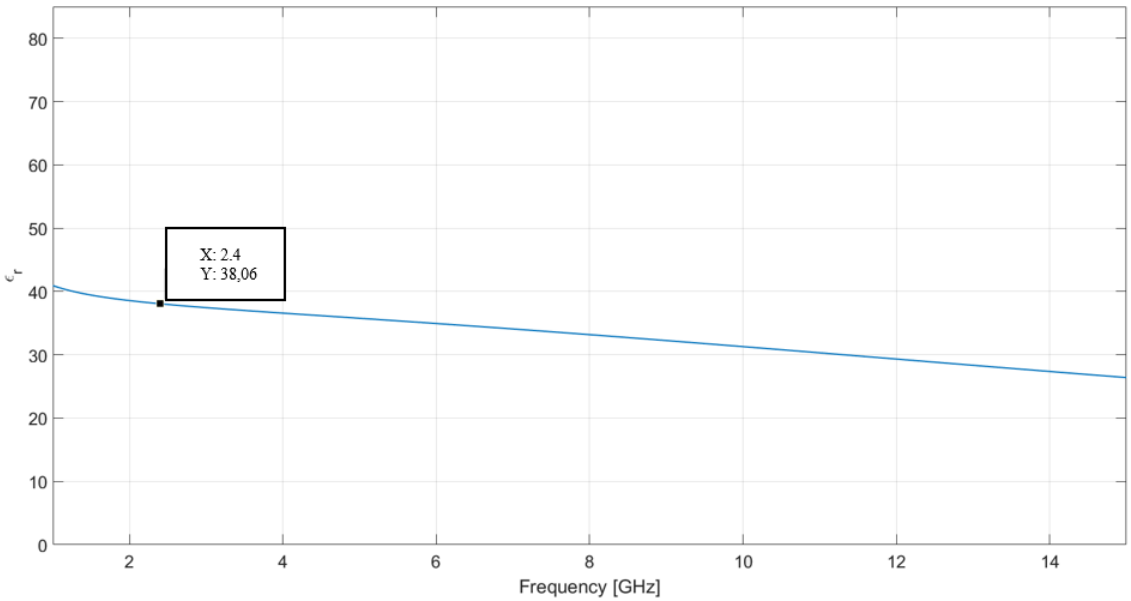

Figure 21 Dielectric constant behaviour of Dry Skin layer.

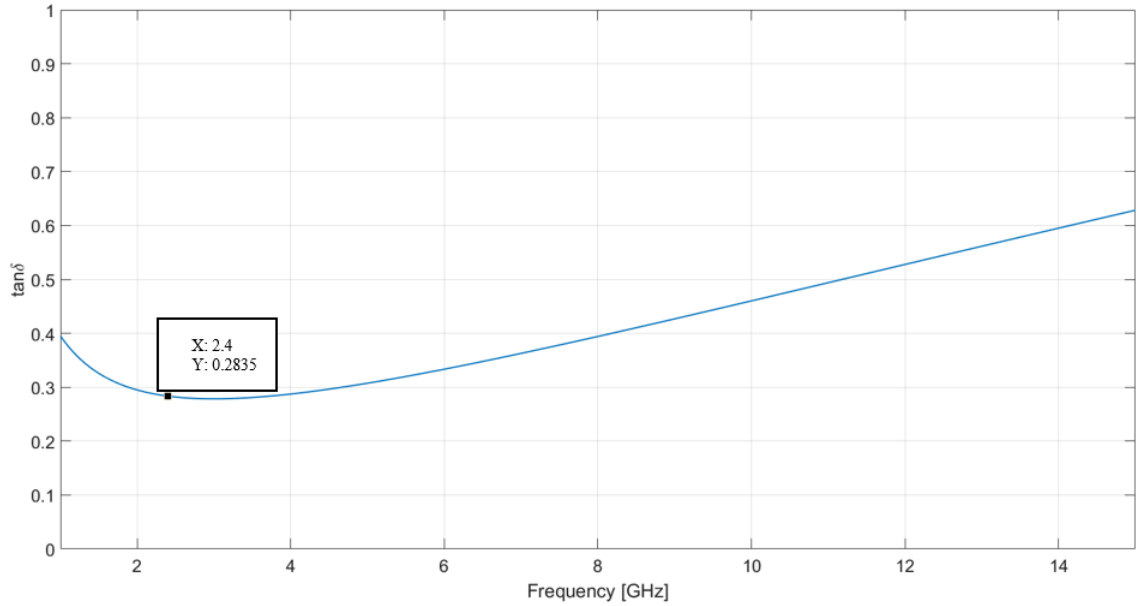

Figure 22 Tangent Loss Factor behaviour of Dry Skin layer.

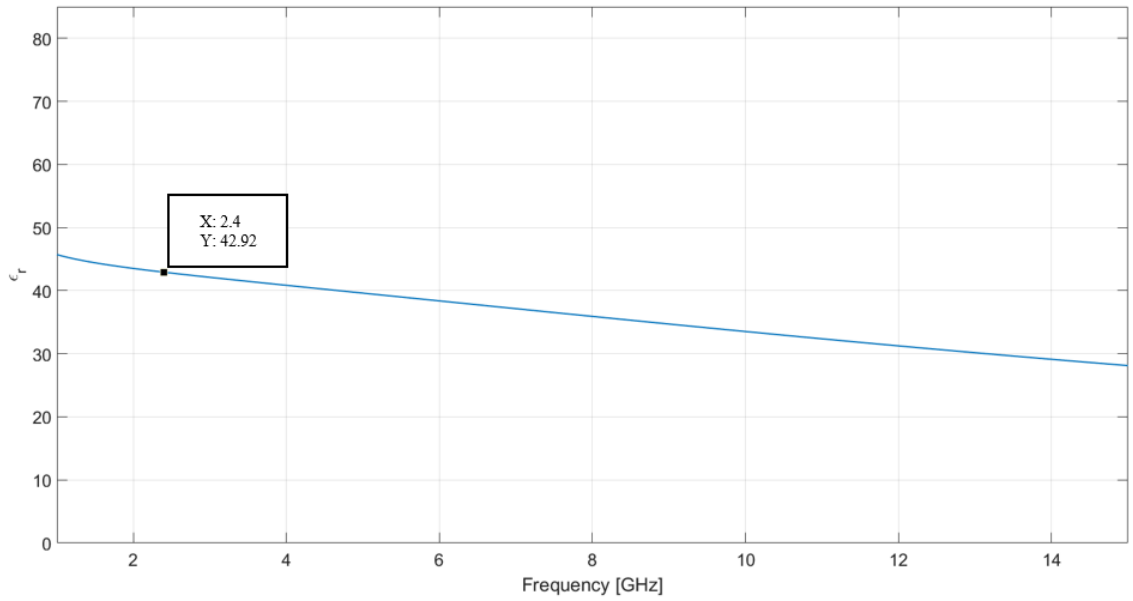

Figure 23 Dielectric constant behaviour of Wet Skin layer.

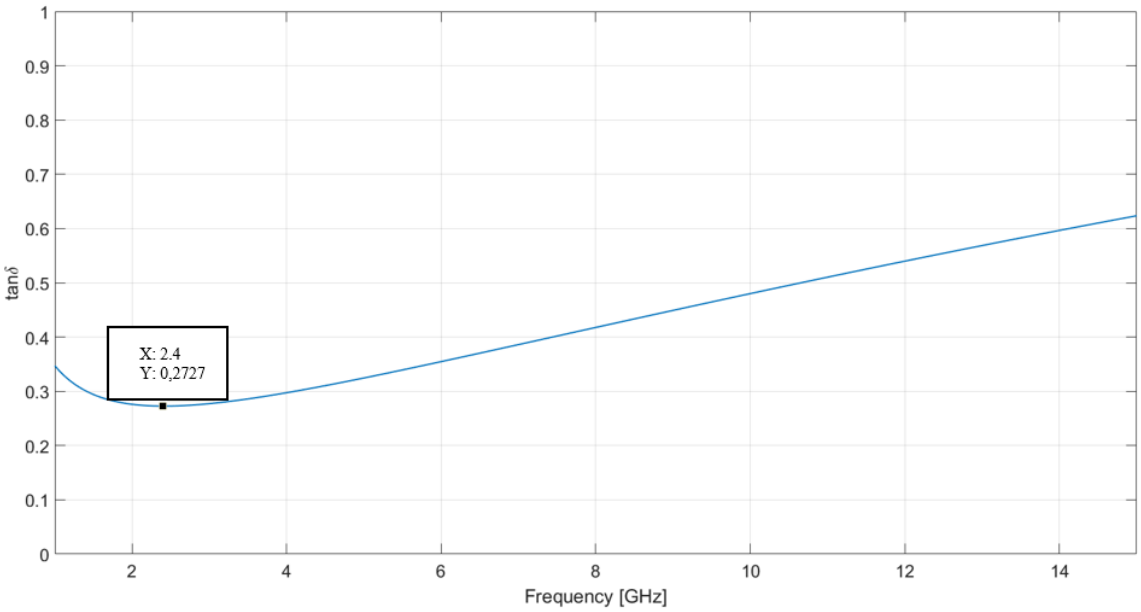

Figure 24 Tangent Loss Factor behaviour of Wet Skin layer.

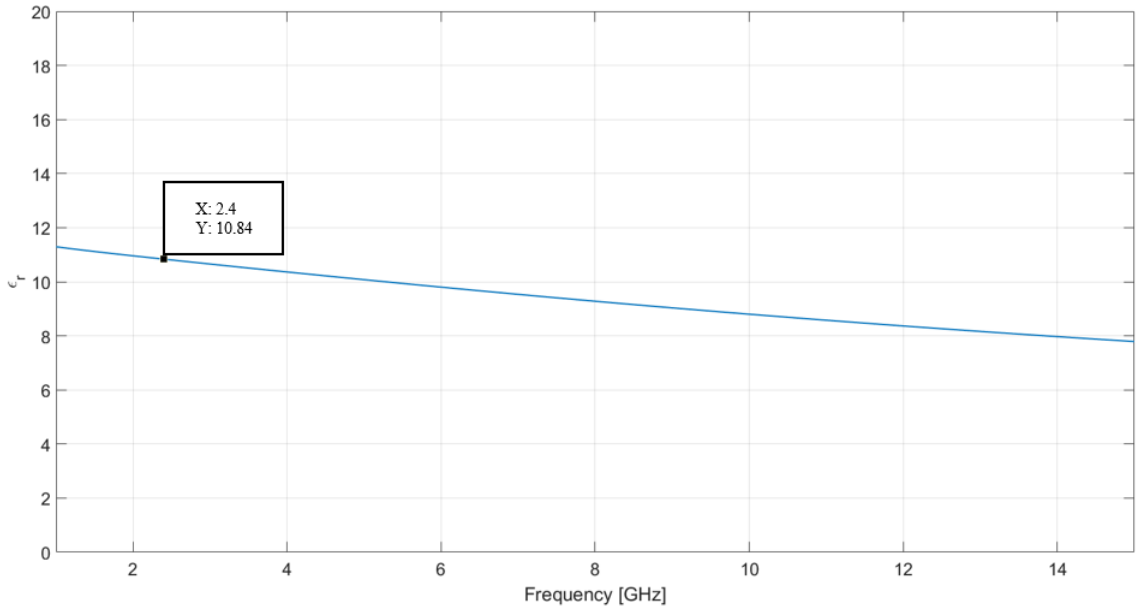

Figure 25 Dielectric constant behaviour of Fat layer.

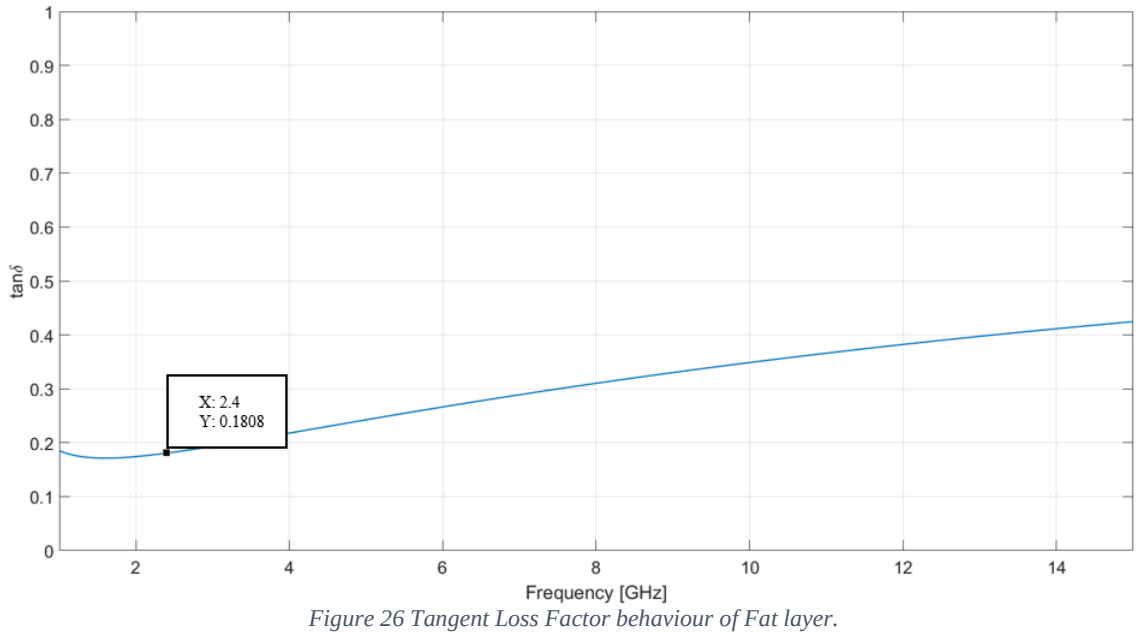

Figure 26 Tangent Loss Factor behaviour of Fat layer.

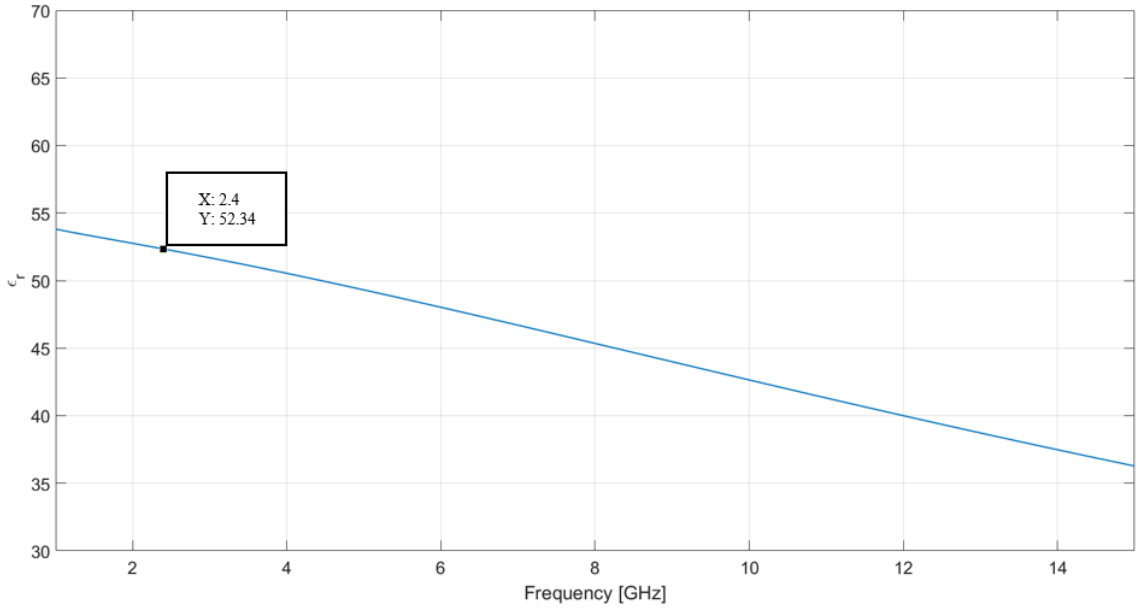

Figure 27 Dielectric constant behaviour of Muscle layer.

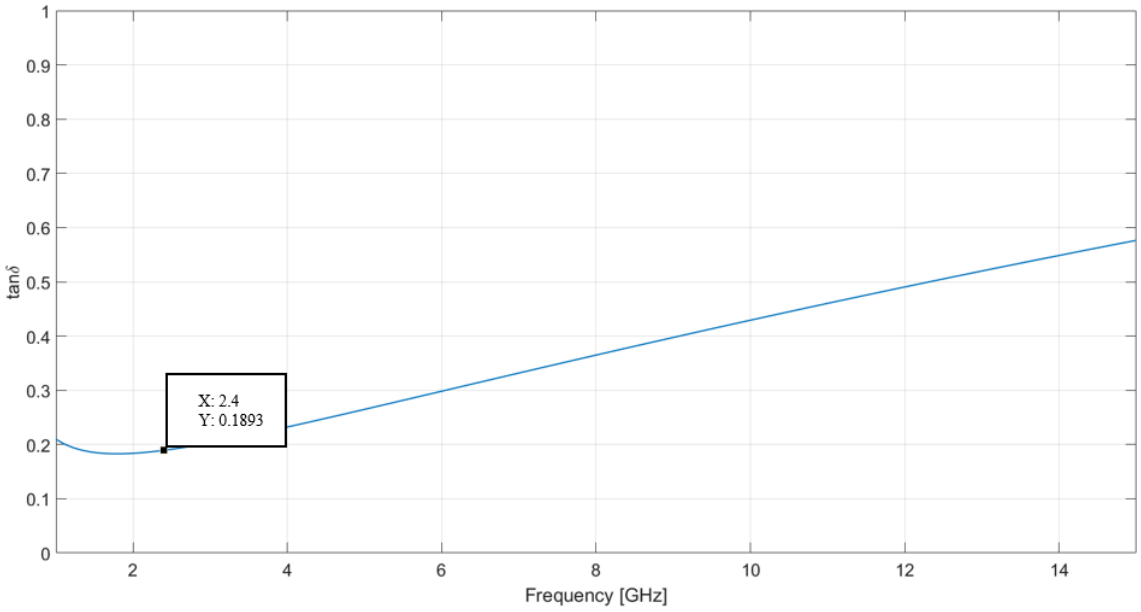

Figure 28 Tangent Loss Factor behaviour of Muscle layer.

4.3.2 Simulations Results on Ansys Software

High Frequency Electromagnetic Field Simulation (HFSS™) from Ansys is a finite element method solver software tool useful for simulating 3D electromagnetic structures. The software can accurately characterize an antenna's performance in free space as well as its performance when modelled surrounded by the human tissue layer, and the effect of the presence of any additional antennas in close proximity. Each human tissue layer is modelled electrically with a corresponding electrical permittivity and conductivity as previously described.

First simulations are performed by assuming the configuration of Fig. 20, with blood dielectric data at various glucose concentrations (BGC) obtained from the model reported in [25]. The relative results, in terms of return loss behaviour vs. frequency (Fig. 29) clearly reveal that the above dielectric model is not effective to predict the variation of the microwave sensor reflection response when varying the BGC.

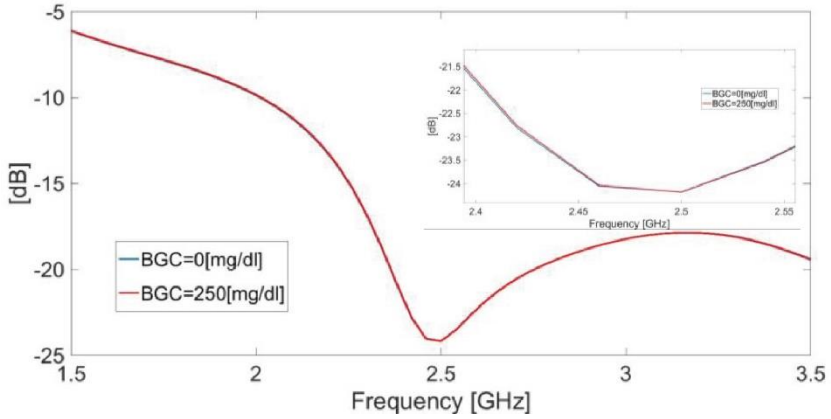

Figure 29 Simulated return loss of configuration in Fig.21, for different BGC (blood dielectric model as given in [25]).

This is probably due to the fact that electrical parameters derived in [25] are retrieved for large span between consecutive values of BGC, namely 0, 250,

500, while near strict values of BGC in the range between 0 and 300 are typically required to be reconstructed by well-working microwave sensors.
As a subsequent step, the dielectric model (11), assuming only the variation of real part of permittivity with respect to BGC is considered, and the relative curves are reported in Fig. 30, where a proper variation of the resonant frequency is approximately modelled.

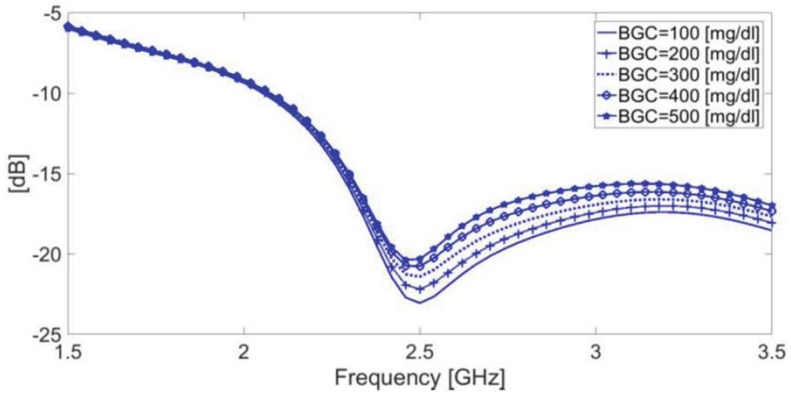

Figure 30 Simulated return loss of configuration in Fig.21, for different BGC (blood dielectric model as given in [26]).

Finally, the enhanced model (26) elaborated in the present work is applied to achieve the simulation results of Fig. 31, where a better accuracy is achieved in terms of return loss amplitude variation vs. BGC, which is typically affected by the loss tangent parameter, properly modelled by the correction factor. The achieved improvement can be appreciated in Fig. 32, where the comparison between the return loss amplitude obtained from the two models at various BGC is reported. It can be easily observed that dielectric model proposed in this work gives higher amplitude variations when changing the BGC, thus revealing a better modelling of the loss tangent effect, and leading to improve the correlation between the reflection response of the microwave sensor and the relative BGC.

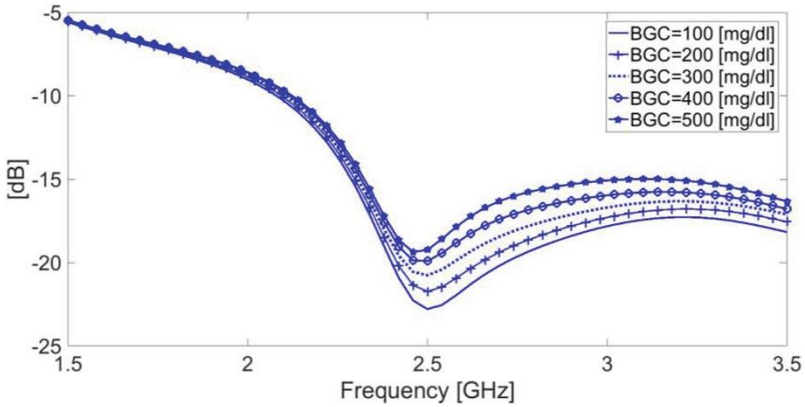

Figure 31 Simulated return loss of configuration in Fig.21, for different BGC (blood dielectric model as given in [30]).

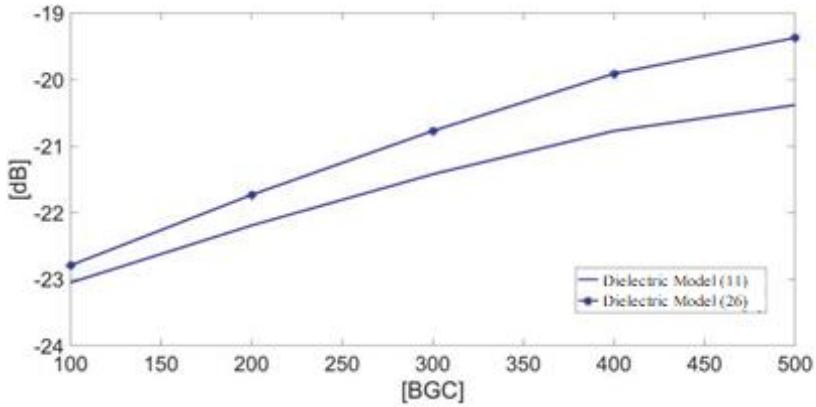

Figure 32 Comparison of return loss amplitude vs. BGC obtained from dielectric models (11) and (26).

This first numerical validation has established the improved accuracy of enhanced model elaborated with respect to existing approaches in literature. This model has therefore become the reference for the rest of the thesis, where, as will be illustrated in subsequent chapters, an attempt has been made to realize a new technology for non-invasive monitoring of blood-glucose levels.

5 SELF-MONITORING OF BLOOD GLUCOSE (SMBG)

Technological development has invaded more and more every aspect of the society by changing and influencing everyone's lifestyle. Even the medicine has not been removed from this digital revolution, in fact, even this sector has undergone radical changes. Starting from the simple data management of the various patients up to the diagnosis and treatment of various diseases, enjoying all the advantages brought by digital innovations. No longer talk about simple medicine, but of *'smart medicine'*, where new technologies are transforming the spaces of health, in particular through the continuous monitoring of people at home, during leisure time and also in the workplace, recording the events that happen. Monitoring of blood sugar is among the procedures that in the recent past have benefited most from technological progress, with the historical objective of continuous monitoring and the prospect of the realization of artificial micro-pancreas, the ultimate goal of technological evolution for function replacement endocrine-pancreatic.

The clinical benefit, intended as risk reduction to develop micro and macro vascular complications obtained by strict glycaemic control in the Type 1 diabetes patients, has been widely demonstrated by the reference studies [32][33].

In these studies, the self-monitoring of blood glucose (SMBG), or the frequent daily measurement of glycaemia by micro-capillary blood sampling with lancing, has been an integral part of the intensive insulin treatment through which it has been obtained better blood glucose control and therefore a reduction in diabetes complications. The importance of SMBG in intensive treatment has been later codified within several recommendations of clinical practice, including those of American Diabetes Association (ADA), [34]. The SMBG remains a tool only in applied part and largely imperfect, in fact,

even today most patients do not perform a reasonable number of SMBG indicated in 3 or more times per day, essentially due to insufficient education, pain associated with puncture, difficulty in reading for some patients, frequent lack of preparation in the interpretation of the results.

Another limitation of the SMBG devices is related to the invasiveness of the instruments on which it is based, which does not allow a continuous analysis over time of the glucose variations in the blood (but only an analysis at intervals of some hours from each other).

The aim of this work, as said, is to overcame the limitations of the standard tools introducing in addition to non-invasiveness also the continuous monitoring.

Some advantages, utility and differences between the two methods (standard SMBG and new approach) are shown below:

1. while the standard SMBG measures glucose levels with good accuracy but sporadically, the devices for continuous monitoring perform a number of surveys to cover the entire arc of the day in a continuous way;
2. with the SMBG measurements the blood glucose trend in the immediate future is not predictable, while continuous monitoring can identify glycaemic trends and consequently offer one predictive ability;
3. the occasional blood glucose measurement requires an active participation of the patient, while the continuous monitoring devices record blood glucose regardless of patient participation.

5.1 Sensor Accuracy

The problem of measuring accuracy of glucose monitoring devices is obviously essential to assess its clinical utility.

An instrument is all the more precise from a point of view analytical, the more the glycaemic value generated by it approaches the value simultaneously generated by the reference tool indicated by the manufacturer (accuracy) and how much closer they are to the values of successive measurements (precision), Fig. 33.

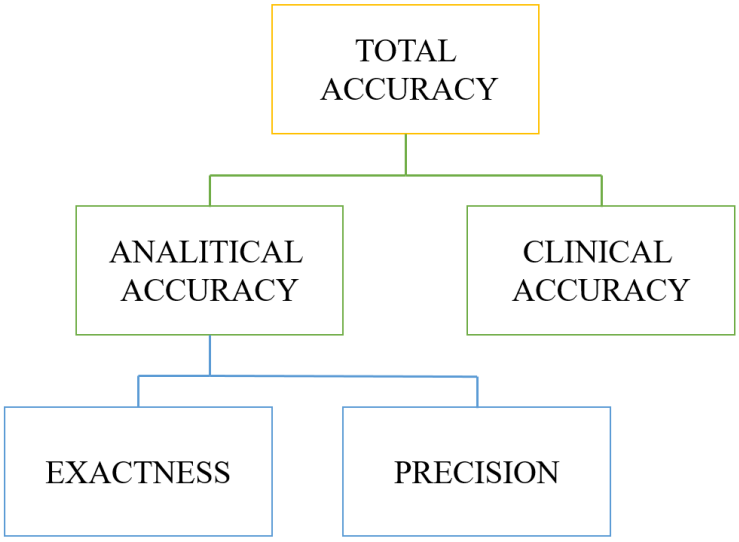

Figure 33 System Accuracy.

The elements that can affect the accuracy of the value of glucose determined on capillary blood is the modality of test execution and the reading system. There are, however, additional elements not strictly related to the procedure or the system that can influence the result (temperature, humidity, altitude, bilirubin, uric acid, et al.).

Innovative systems use detection principles of signal, which allow to correct the influence on the glycaemic data within certain limits from any external interfering factors, thanks to sophisticated algorithms. Having an accurate

tool means, in the short term, to be able to make the right decisions, for example inject the appropriate dose of insulin before a meal or take a certain amount of carbohydrates in case of low blood sugar levels. In the long term, it means being able to propose to each patient self-monitoring structured with the purpose of interpret the progression of blood sugar levels at different times of the day and at the same time make decisions therapeutic.

In recent years, international regulatory authorities (International Organization for Standardization, ISO), in order to guarantee a higher quality of glycaemia sensor, have defined new rules that, only if respected, allow a company to define its own accurate product and to obtain the CE marking for placing on the market. The new regulation **ISO 15197: 2013** (which has supplanted that of the 2003) provides that for blood glucose values <100 mg/dL, the values generated by the meter must vary to the maximum of ±15 mg/dL compared to the values obtained with the method of reference, while for values ≥ 100 mg/dL the values glycaemic drugs generated by the glucometer must vary to maximum of ± 15% with respect to the generated value from the reference method. In practice, if the real value determined with the reference method is 90 mg/dL, the sensor in order to be accurate must generate a value which is between 75-105 mg/dL. If the value real is 200 mg/dL, the glucometer to be called accurate must generate a value that is between 170-230 mg/dL.

However, not only the "quality" of the data is important, and that is, if the data from the self-monitoring system approaches to the reference datum, but also the "quantity" and that is how many times on a sufficient number of determinations the data generated by the system approach or move away from the real one. In detail, the rule provides that the system is sufficiently accurate if, on a number set of determinations (100 measurements for two different glucometers for three different lots = 600), tolerance predicted for values <100 mg / dL and ≥ 100 mg / dL is respected in both conditions in at

least 95% of cases. Specifically, if 100 determinations are made of blood glucose respectively with self-monitoring and with reference method, at least 95% of cases are blood glucose levels obtained through self-monitoring must comply with the rule of ± 15 mg / dL per blood glucose values <100 mg / dL and ± 15% for values ≥ 100 mg / dL. The 100 tests performed must include samples with glycaemia distributed between values between <50 and >400 mg/dL according to a well-defined proportion in the standard itself.

So far the analytical accuracy of the systems, more closely related to technical features, but equally important is accuracy clinical, or the clinical impact it may have a system when used to make therapeutic decisions. The Clarke grid is the representation mode graphic of clinical accuracy. The grid represents the probability of making a decision correct therapy based on the value obtained with the system self-monitoring. It identifies 5 different areas (A-E) of clinical risk, which fit into a system of axes that illustrates the concordance between blood glucose obtained with self-monitoring and that obtained with the reference standard. There is a more grid stringent for type 1 diabetes and a less stringent one for type 2 diabetes. ISO 15197:2013, however, it refers only to type 1 diabetes and establishes that 99% of the measurements must fall into the zone A and B. This additional rule, not present in the 2003 version, guarantees greater security for those who need to adapt daily insulin dose based on blood glucose value. Values glycaemic drugs that fall into zone A and B allow for make clinical decisions especially safely thanks to the good and fair accuracy of the data glycaemic. On the contrary, the glycaemic data that are placed in areas C, D, E could lead to take of inadequate and even dangerous clinical decisions for the patient, Fig. 34, [35].

A simple example can help to better understand the danger of having a system self-monitoring whose determinations may fall in areas C to E of the grid. A

blood sugar obtained with self-monitoring of 150 mg/dL which falls in zone C it will correspond to a real value between 70 and 50 mg/dL.

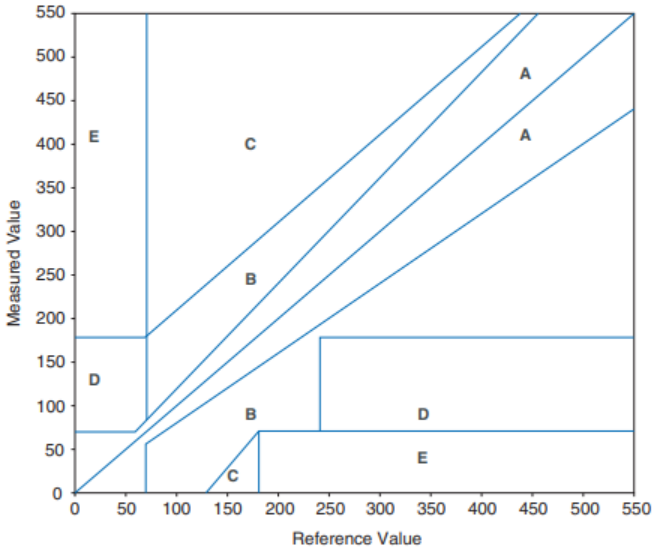

Figure 34 The Clarke error grid.

Similarly, a blood glucose of 50 mg/dL that always falls in zone C will correspond to one real blood sugar between 120 and 250 mg / dL. In the first case, a subject with asymptomatic hypoglycaemia may not take any initiative and make your condition worse of hypoglycaemia. In the second case a subject could take carbohydrates thinking to correct asymptomatic hypoglycaemia, worsening furthermore a situation of hyperglycaemia.

Commonly speaking of accuracy, reference is made on the grill of Clarke, while rarely the data of **MARD (Mean Absolute Relative Difference Percentage**) that are used instead for interstitial glucose reading systems (Continuous Glucose Monitoring and Flash Glucose Monitoring). MARD (%) indicates the discrepancy between the glycaemic value determined with the reading system and the value determined with the reference standard. In practice, the absolute difference between the first is calculated two glycaemic values and then the percentage difference.

MARD is expressed as an average value over a sufficient number of observations.

6 WEARABLE ANTENNAS OVERVIEW

Wearable antennas have been a topic of interest for more than the past decade, and hundreds of scientific papers can be found on the topic. This large number of publications asks for some classification in order to get an overview of the trends and challenges.

The main classification to be done is that of applications, therefore the three macrocategories in which the wearable antennas are applied will be described below.

1. **Security and Rescue Service Applications**

These wearable antennas intended to operate in various harsh environments. These antennas are mainly used for security and defence applications [36] and within different rescue services like firefighters [37], mountain and water rescue workers [38].

Frequency bands intended for security and rescue applications is the Tetrapol communication band, 380-430 MHz, widely used by different security and emergency services within the Private Mobile Radio (PMR) applications.

There are two common requirements for most of the wearable antennas used in security and rescue service applications: the size miniaturization and the resilience of the antenna to the environment.

Antennas used for these applications should be small, non-protrusive, low profile and conformable so that can be easily mounted inside the uniform and placed around the wearer's body.

Apart from the antenna size, another important aspect is the environment and weather conditions where wearable antennas operate. As most of the wearers from the indicated groups operate outdoor, robustness against water, rain, moisture, mud, etc., is among the antenna requirements. Moreover, taking

into account that the uniforms need to be washed an integrated antenna should withstand this process.

Several antenna prototypes exist in literature and on the market [39][40][41]. All the reported antennas have a size suitable for placement on the wearer. Some of the antennas are waterproof and most of them are specific and customized and cannot be widely used for different situations. Different parameters can be monitored with the antennas integrated in their garments like psychological parameters, actual position or the conditions on the field where they operate.

In summary, all the concerned applications, such as military, fire fighters or rescue services, require an involvement of different electronic devices and equipment in their daily activities. Depending on the type of application and activities they perform, different wearable antennas are needed. Therefore, wearable antennas play an important role in ensuring robust and reliable communication links and thus performance of these services.

2. Sport, Entertainment and Fashion Applications

Another attractive market for wearables is sport, entertainment and fashion applications. Nowadays consumers enjoy keeping track of performances in any kind of sports activity they do. Different wearable applications are able to track and record speed, elevation, distance and other similar parameters. Most of the tracking can be performed with the currently existing smart phones, but some separate wearable devices also exist Wearable GPS antennas, [42][43], play important role in performance of such systems. Furthermore, for the purposes of professional sportsmen, wearable devices are used in a more extensive manner. All the collected data from different wearable sensors are analyzed and used for further improvement for the sportspeople performances [44].

Other interesting examples of wearable antennas intended for integration into the shoes and thus potential use for sports applications are presented in [45][46].

Entertainment applications is also a market for the wearable technologies. They offer a lot of possibilities to this industry.

Some examples of entertainment wearables present on the market, include Bluetooth jacket [47], intelligent shoes [48] or ski monitoring system.

3. Medical Applications

Medical applications consume large portion of the WBANs [49]. These applications are mainly used for health monitoring of different categories of patients and elderly people. They can monitor 24 hours a day different parameters and detect changes, for instance blood pressure, heart rate or body temperature [50], Fig. 35. With the more emphasized use of smart phones, collected data from the medical applications can be directly sent to the hospital or responsible medical doctors [51].

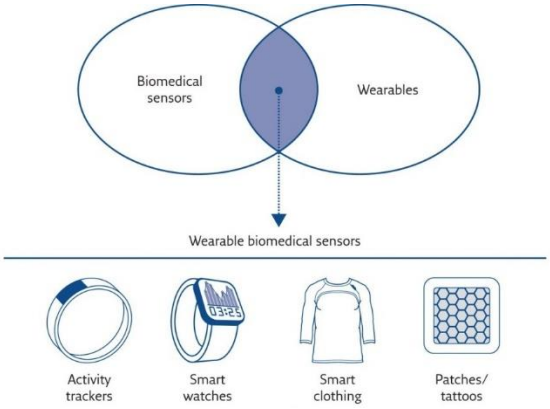

Figure 35 Wearable biomedical sensors.

Depending on the type of devices (implanted or on body) and the required communication (In-, On- or Off-body) different standards have been defined. The Federal Communications Commission (FCC) has established a Medical Implant Communication Service (MICS) like the band for communication with medical implants, while in Europe the same standard is regulated by the

European Telecommunications Standards Institute (ETSI). In 2009, the Medical Device Radio Communications Service (MedRadio) range, 401-406MHz, has been created by the FCC for diagnostic and therapeutic purposes in implanted medical devices and devices worn on the body.

Large number of wearable applications operate inside one of the FCC proposed Industrial Scientific Medical (ISM) bands, 902-9281 MHz, 2.4-2.4835 GHz and 5.725-5.875 GHz. Some of the bands are used on a secondary basis because they are already utilized in other applications.

These ISM bands are submitted to certain restrictions, like short distance operation or low emitted power, in order to allow their co-existence in the spectrum with minimal interference.

The large choice of frequency bands used for medical WBAN applications leads to various wearable antenna families. Several implantable and wearable antennas are presented within the following subsection.

The antenna needs to be small, compact, built out of appropriate bio-compatible materials and when implanted providing a reliable communication link towards the external units and devices. Medical applications will remain one of the main consumers of various wearable devices. Constant progress of the wearables allows monitoring of various health activities and parameters.

In the next paragraph, the design phases of a new wearable device for continuous and non-invasive monitoring of blood glucose levels have been presented. The principle of operation and the results of experimental measurements will also be discussed.

6.1 Wearable Textile Antenna for Contactless Blood-Glucose Monitoring

One of the most widely used methods for making microwave-based biosensors is the resonator method. The resonator method is based on the fact that the resonant frequency and quality factor of a dielectric resonator with given dimensions are determined by its permittivity and permeability. For a resonator with given electromagnetic boundaries, when part of the electromagnetic boundary condition is changed by introducing a sample, its resonant frequency and quality factor will also be changed, from these changes, the dielectric properties of the sample, in the specific case of the thesis the blood dielectric parameters, can be derived. The material under test is either part of the resonator (the resonator method) or is in the proximity of the resonator (the resonant-perturbation method) [52].

In this chapter the design of the bio-sensor for non-invasive and contactless monitoring of blood glucose levels will be reported. After choosing the materials to be used, the choice of the antenna configuration and its design will be discussed. The tests carried out on the sensor realized will also be reported and commented.

In addition to assessing the frequency response of the antenna, the levels of SAR reached by the antenna will also be discussed, given its operation in close contact with the human body.

6.2 Textile Materials Chosen for the Biosensor

The substrate material plays a fundamental role in the design and fabrication of antennas. In particular, in the case of wearable antennas, the integration of the antennas into the daily clothing indirectly imposes the potential choice of conductive and substrate materials. A wide range of materials can be found

in the literature: textiles, specially treated yarns, printed conductors, polymers [53].

An additional reason why a careful selection of the materials should be considered is the operating environment that influences the performances of the antenna. Apart from the body's influence on the antennas, they can be also exposed to different harsh environment, manifested through different weather conditions like rain, humidity, snow, mud or ice.

Textile materials are among the most deployed materials for building wearable antennas. They are light weight and can be easily integrated in the wearer's garments.

These materials are planar fibrous materials which properties are mainly determined by the properties of the component fibres. They are porous materials, in which the density of the fibres, air volume and size of the pores determine general behaviour, for instance, air permeability and thermal insulation. Accordingly, fabrics are flexible and compressible materials which thickness and density might change with low pressure.

Obviously for the realization of a wearable antenna it is necessary to have two different materials, a dielectric for the substrate and a conductive one for the patch, the ground plane and for all the other conductive parts.

Furthermore, the materials used for the radiating patch and the ground plane need to have good conducting characteristics and low losses, while the dielectric material should have constant thickness and low loss dielectric permittivity.

An overview of the conductive materials is reported in [54]:

- *Conducting Ribbon*: this is a commercially available product consisting of typically 3-6 tracks of conductive thread woven into a non-conductive backing ribbon fabric.
- *Insulated Wire:* this is a standard flexible insulated wire which is an ideal candidate for the broadband dipole.

- *Conducting Paint*: these materials are consisting of high silver content to produce a low electrical resistance.
- *Conducting Nylon*: material available from a variety of manufacturers.
- *Conducting Thread*: material suitable for spiral antennas.
- *Screen Print*: easy way to write a pattern on some textile.
- *Coated Copper Fabric*: there are a variety of commercial processes available to coat fabric with copper.

The choice of dielectric materials is larger compared to the conductive ones. Simply, most of the textiles have low relative permittivity and relatively low tangent loss factor, thus making them suitable substrates for wearable antennas. Since no additional fabrication treatments are required, theoretically most of the textiles can be used as substrate materials. The Table 9, presents the different dielectric materials found among the wearable applications, showing their thicknesses and the electrical characteristics (relative permittivity and tangent loss factor).

Table 9: Possible dielectric material to use for substrate.

Material	**Thickness [mm]**	**ε_r**	**tanδ**
Felt	1.1	1.38	0.023
Woolen felt	3.5	1.45	0.02
Polyamide fabric	6	1.14	Negligibile
Fleece	2.56	1.25	Negligibile
Closed-cell foam	3.94	1.52	0.012
Silk	0.58	1.75	0.012
Tween	0.68	1.69	0.008
Panama	0.437	2.12	0.018
Moleskin	1.17	1.45	0.05
PTFE	11.66	2.05	0.0017
Denim	1	1.7	0.025

After this overview on textile materials that can be used for substrate and conductive parts, in the following chapter the design of the wearable and

textile antenna for non-invasive monitoring of glucose levels will be discussed.

Before proceeding with the analysis of the steps carried out for the sensor design, it is advisable to define the textile materials used for the conductive parts of the sensor and for the substrate. For this project, the chosen textile substrate is a standard *denim*, Fig. 36, which is durable, inelastic, low thickness, comfortable for user and low-cost.

Figure 36 Standard fabric denim.

Firstly, its electromagnetic properties have been measured in the μwave Laboratory at the University of Calabria. The thickness considered is equal to 2 mm, Fig. 37.

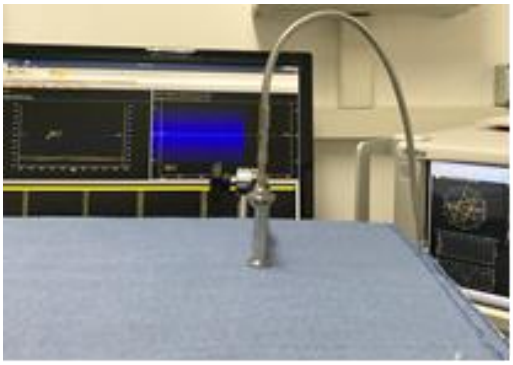

Figure 37 Photograph of setup for dielectric characterization of denim substrate (Microwave Laboratory at University of Calabria).

The result of the electromagnetic characterization is reported in Table 10.

Table 10: Dielectric characteristics of denim at 2.45 GHz.

Material	Thickness [mm]	ε_r	tanδ
Denim	2	1.6	0.01

The choice of frequency equal to 2.45 GHz will be discussed later.

If denim has been employed for the substrate, another fabric with very special characteristics has been chosen for the conductive parts (conductive radiator and ground plane), the PCPTF (*Pure Copper Polyester Taffeta Fabric*).

The selection of an appropriate conductive textile is an important step in the design of a textile antenna. Properties of PCPTF are given in Table 11.

Table 11: Properties of PCPTF used for the wearable antenna.

Properties	PCPTF
Surface Resistance	0.05 Ohm/sq
Conductivity	$2.5x10^5$ S/m
Thickness	0.08 mm
Weight	80 g/m^2

PCPTF is made using 35% of copper and has the advantages of being flexible, light weight, easy to be cut, sewn and meant to be used in electromagnetic shielding applications.

6.3 Frequency Band Selection

The selection of the available frequency bands is regulated by the frequency allocation plans published by government offices. Specific frequency bands indirectly can determine the size of the antenna and influence the choice of the configuration type. Too low frequencies would result in large antenna structures that would be hard to integrate on the user's body, whereas too high frequencies would result in very small structures sensitive to fabrication tolerances, leading to the increase of the fabrication costs.

The International Telecommunication Union (ITU), which is the United Nations (UN) specialized agency for information and communication

technologies (ICTs), allocates the global radio spectrum and develops different technical standards [55].

Electromagnetic wave propagation is strongly linked to the frequency, where the wavelength determines the size of the obstacles or transmission medium that will mostly influence the wave and its propagation. For frequency ranges from a few Hz up to several GHz, THz or higher, the size of the wavelength goes from several km down to a few nm, respectively. Table 12 shows several radio wave bands.

Table 12: Radio Spectrum.

Band	Frequency	Wavelength
Very Low Frequency (VLF)	3-30 kHz	100-10 km
Low Frequency (LF)	30-300 kHz	10-1 km
Medium Frequency (MF)	300-3000 kHz	1-0.1 km
High Frequency (HF)	3-30 MHz	100-10 m
Very High Frequency (VHF)	30-300 MHz	10-1 m
Ultra High Frequency (UHF)	300-3000 MHz	100-10 cm
Super High Frequency (SHF)	3-30 GHz	10-1 cm
Extremely High Frequency (EHF)	30-300 GHz	10-1 mm

According to the Table 12, three frequency bands are possibly seen as appropriate solutions for Body-Worn antennas, VHF, UHF and SHF band. The sizes of the antennas operating at those three bands are convenient so that they can be easily placed on the wearer's body. Frequency bands lower than VHF are not good since their wavelengths are longer than 10 m and they are usually used for very long distances. On the other end of the frequency spectrum, EHF band faces the problem of traveling of such waves across most of the obstacles like walls, trees, buildings, and even the atmosphere. The smaller the wavelength is, the more interference with small objects appears, at some point even interfering with molecules.

The frequency chosen for the design of the wearable sensor of this work is 2.4 GHz. This frequency is also part of the **ISM-band** that was originally internationally dedicated for RF electromagnetic fields for **Industrial**, **Scientific** and **Medical** purposes.

2.4 GHz is the most common because there is no need for licensing devices to use it. Other ISM frequencies can be as high as 24.125 GHz or even as low as 13.56 MHz depending on the location and local acceptance, authorities can allocate ISM radio frequencies with some little flexibility.

6.4 Biosensor Configuration

The antenna configuration for the designed wearable sensor is a standard coaxial probe fed patch antenna, Fig. 38, [56].

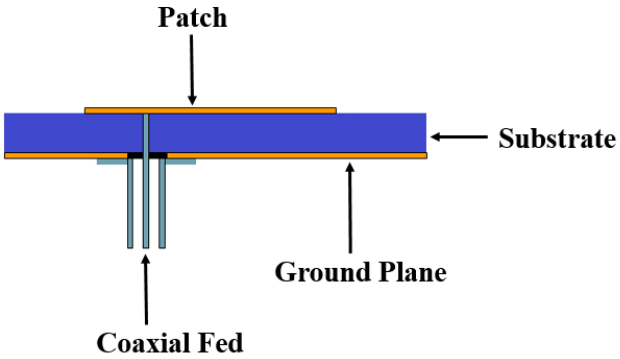

Figure 38 Cross section of microstrip patch antenna.

The microstrip patch is a planar antenna, consisting of a radiating patch on one side of the dielectric substrate, and the ground plane on the other. The radiating elements are made of conducting materials (e.g. copper, usually photo-etched). Patches can be found in any geometrical shape, but the most common have some regular shapes as square, rectangular, circular, triangular and elliptical. The microstrip patch is a candidate for any narrowband wearable application, as it has a low profile and can be made conformal for

integration into the clothing, furthermore also the choice of coaxial fed has been made with a view to greater integration with daily clothing.
As previously said, denim has been used for the substrate and PCPTF for the patch and the ground plane.
In the next paragraph, the design steps will be deepened and discussed.

6.5 Wearable Textile Sensor Design

The antenna design was carried out on the CST Studio Software [57]. The antenna designed must work at 2.4 GHz (ISM-Band), Fig. 39.

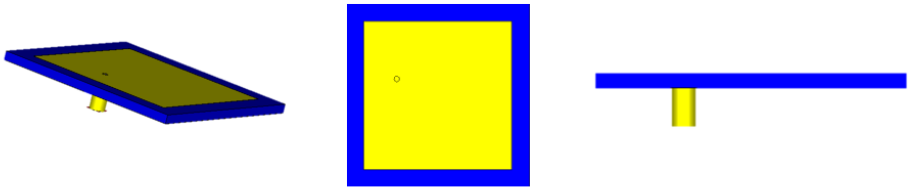

Figure 39 Sensor view on the CST Studio Software.

Initially the antenna has been designed to work in air at 2.4 GHz. The thickness substrate considered is equal to 2 mm.
In order to comply with the project specifications, a tuning has been performed on the physical dimensions of the sensor and on the positioning of the fed.
The shape chosen for the patch is the square one and the first tuning has been performed right on its dimensions. In the Fig. 40, is reported the variation of the resonance frequency when the size of the patch side changes.

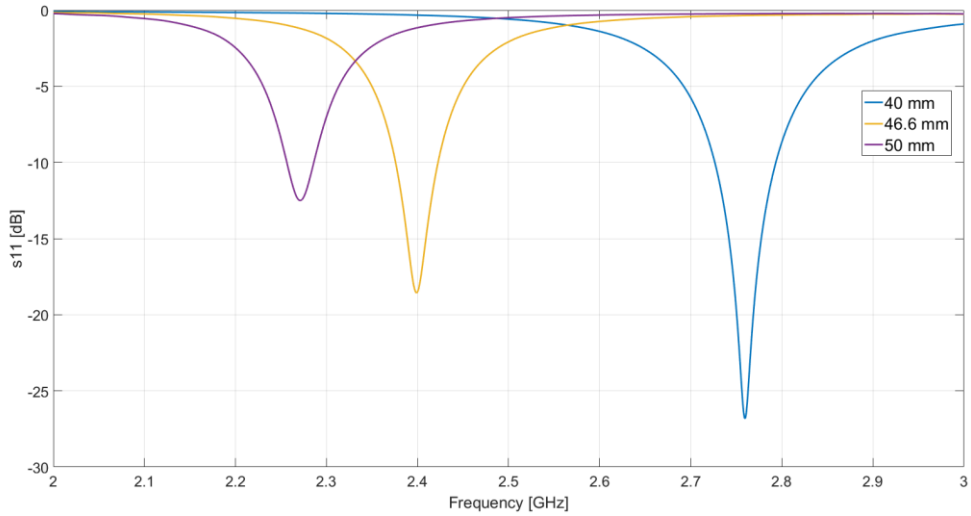

Figure 40 Simulated data showing variation of S11 based on the patch size variation.

After this first tuning on the patch size, it continued changing the ground plane size and the fed position in order to obtain the best possible result in the air.

Radiation pattern has been simulated and the result is reported in Fig. 41.

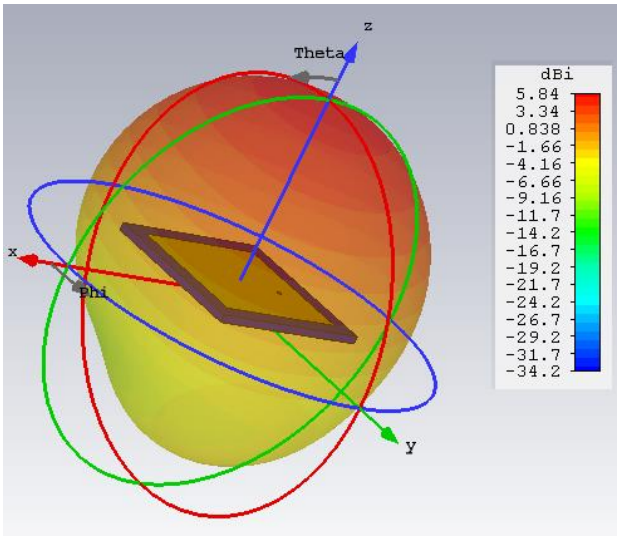

Figure 41 3d View of simulated radiation pattern.

The final sensor dimensions obtained are reported in Fig. 42.

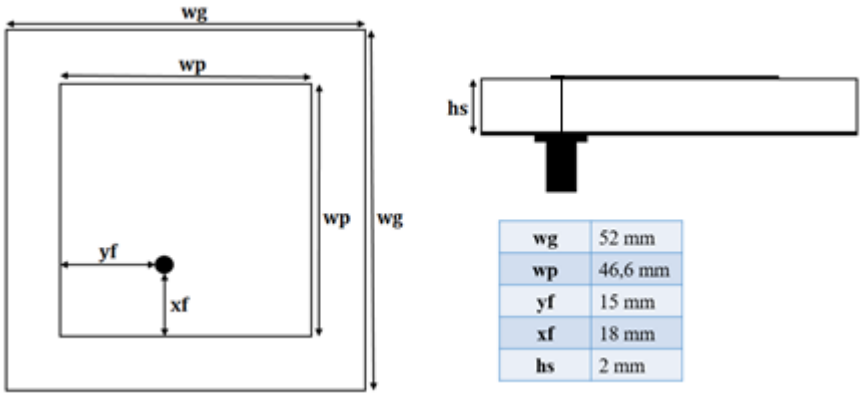

Figure 42 First sensor designed geometry (image not in scale).

Obviously this first prototype, initially designed in the air, will have to work in close contact with the biological tissue, given the required application. For this reason, the following paragraph will show the steps taken to optimize the operation of the wearable sensor in contact with a virtual biological phantom.

6.6 Wearable Textile Sensor in contact with Virtual Biological Phantom

The virtual biological phantom is already reported in Fig. 20. The new configuration designed on the CST Studio Software is reported in Fig. 43, [58].

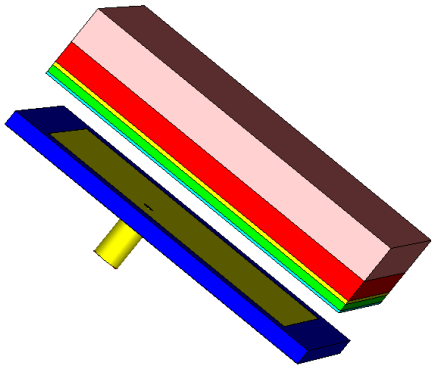

Figure 43 Wearable sensor in contact with virtual biological phantom.

The passage from the air to the biological medium meant that the dimensions initially obtained should be slightly modified. in this perspective it also tried to miniaturize the sensor dimensions as much as possible, to make it as easy to integrate with everyday clothing.

For this reason, a tuning was carried out mainly on the patch and ground dimensions, leaving the substrate thickness equal to 2 mm. The new geometry is reported in Fig. 44.

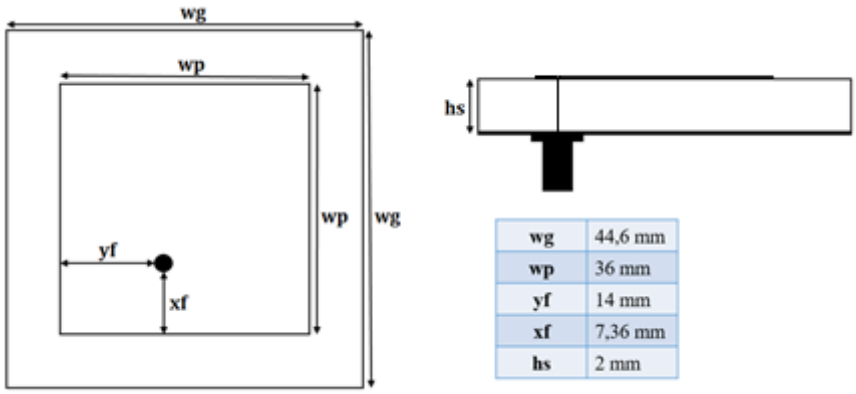

wg	44,6 mm
wp	36 mm
yf	14 mm
xf	7,36 mm
hs	2 mm

Figure 44 Wearable sensor geometry in contact with virtual biological tissues.

Obviously, also the fed position was modified to obtain a correct functioning. The return loss simulated, in this case, is reported in Fig. 45.

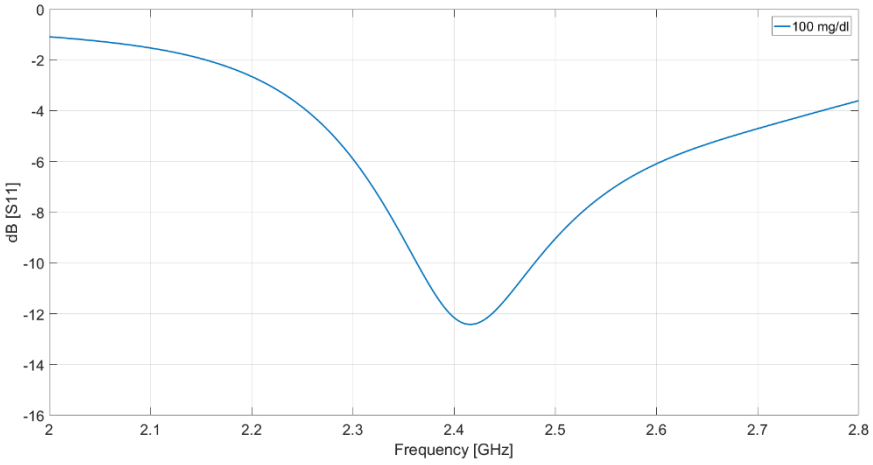

Figure 45 Return loss simulated with the new dimensions.

Instead, the biological superstrate configuration considered is reported in the Table 12.

Table 12: Dielectric properties and thicknesses of the digital phantom considered @2.4 GHz.

Medium	**Thickness [mm]**	**ε_r**	**tanδ**
Dry Skin	0.015	38.06	0.2835
Wet Skin	0.985	42.92	0.2727
Fat	0.5	10.84	0.1808
Blood	2.5	58.53	0.1743
Muscle	10	52.34	0.1893

The dielectric properties of the blood layer have been calculated using the enhanced model proposed in [30], and a reference concentration has been chosen equal to 100 mg/dl. Instead, for the other layers has been used the standard Cole-Cole model [23].

6.7 Wearable Textile Sensor for Contactless Blood-Glucose Monitoring

After verifying the correct functioning of the textile sensor in contact with a biological superstrate, the next step was to vary the glucose concentration in the blood layer in order to evaluate the sensor's efficiency in perceiving BGC variations.

The choice of glucose concentrations to be considered was based on the typical blood glucose values of both a healthy person and a person suffering from diabetes (Table 5).

For this reason, in order to validate wearable sensors some numerical validations are conducted simulating the return loss at different BGC values, with the complex permittivity of blood derived from the enhanced dielectric model [30].

The dielectric constant and tangent loss factor behaviours obtained are reported in Fig. 46 and Fig. 47.

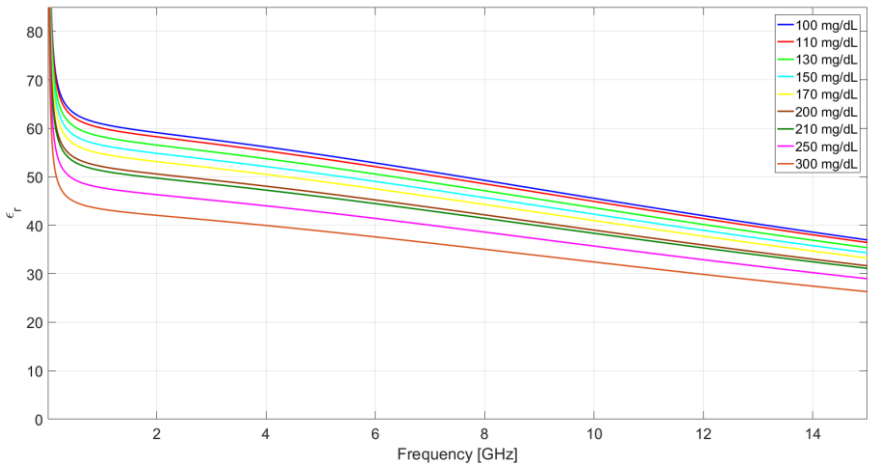

Figure 46 Dielectric constant behaviour at specific BGC values.

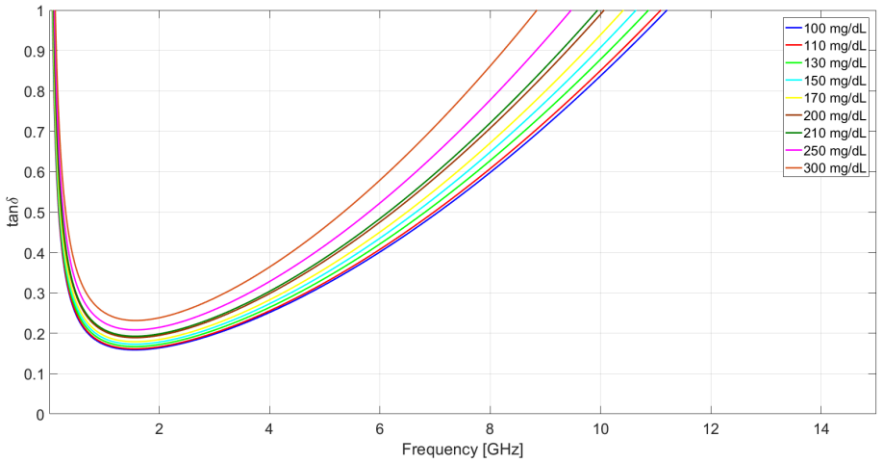

Figure 47 Tangent loss factor behaviour at specific BGC values.

From these curves have been extrapolated the dielectric characteristics of solutions with different glucose concentrations at the frequency equal to 2.4 GHz. These values are reported in Table 13.

Table 13: Dielectric characteristics of blood-glucose solutions @2.4 GHz.

BGC [mg/dl]	ε_r	tanδ
100	58.53	0.1743
110	57.68	0.1772
130	55.99	0.1831
150	54.31	0.1895
170	52.62	0.1962
200	50.08	0.2072
210	49.24	0.211
250	45.86	0.2281
300	41.64	0.2072

The range of variation of BGC, therefore, is a very realistic range for diabetes patients who need to monitor their blood sugar levels daily.

The computed return loss curves, reported in Fig. 48, reveal an evident frequency shift when changing the blood glucose concentration.

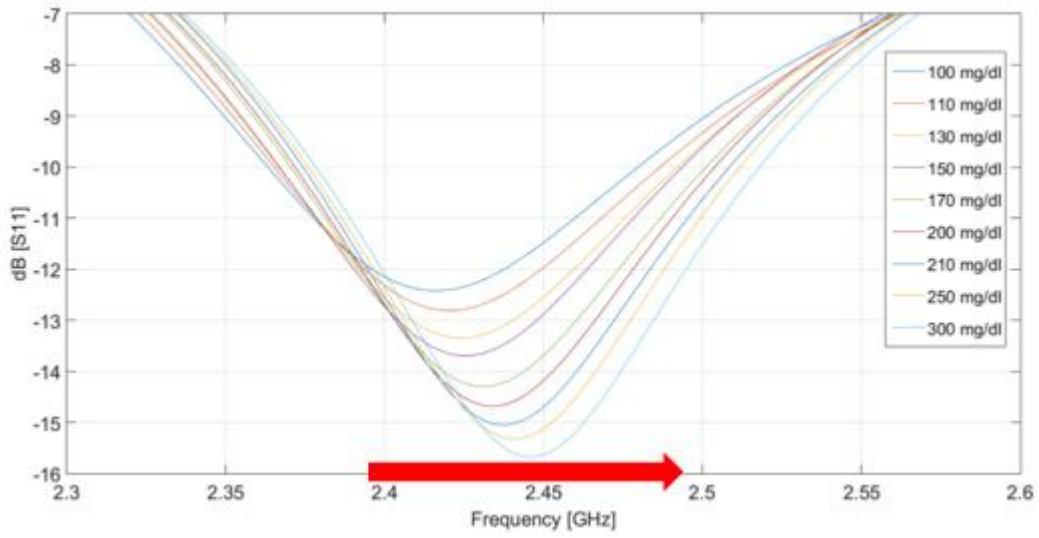

Figure 48 Simulated Return Loss at different BGC for the proposed wearable sensor.

In particular, in Fig. 49, is reported the frequency shift when changes the BGC.

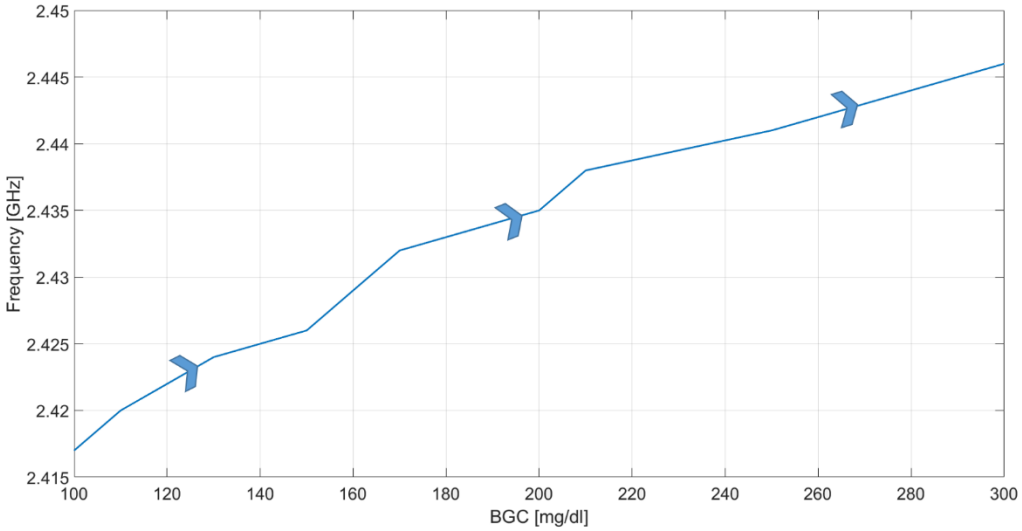

Figure 49 Frequency shift of the return loss for different BGC values.

From the curves shown in Fig. 48, it was possible to derive a two-variable function that would allow the calculation of the BGC (in mg/dl) starting from the resonance frequency (in GHz) and the s11 amplitude (in dB).

$$BGC = \frac{\left(0.6555 \cdot \frac{\omega}{2\pi}\right) + (-0.005616 \cdot s11Amp) - 1.6374}{0.0002} \cdot \left[\frac{mg}{dl}\right] \quad (27)$$

This function reconstructs fairly precisely the concentration of glucose in the blood, it is clear that to increase its accuracy it is possible to optimize the curve fitting performed by increasing, for example, the number of starting points.

6.8 Parametric Study on the Performances of Wearable Textile Sensor in Contact with Biological Tissues

In this section, the fat and muscle thickness will be modified and the sensor response will be verified. In the previous paragraph, Fig. 48 shows a correct operation at the frequency established with the superstrate values shown in

Table 12. The thickness values reported in the table are average values, it is clear that in reality in many cases they can also vary a lot, for this reason it is very important to have an idea of how the sensor works even in other conditions than the ideal ones. In the Fig. 50, is reported the variation of the resonance frequency when the muscle thickness changes, while in Fig. 51 it is reported what happens when changes the fat thickness. Only these two tissues have been considered as they are the most variable from person to person.

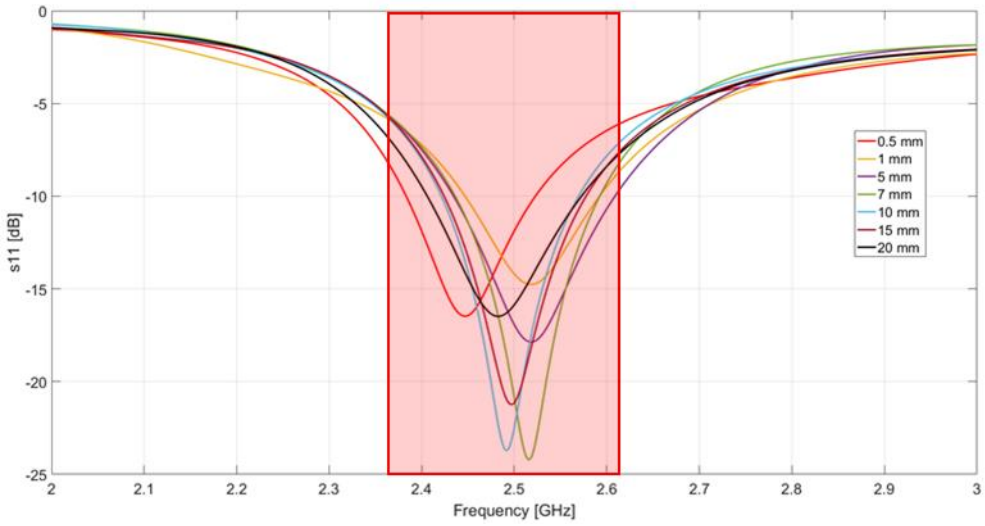

Figure 50 Sensor frequency response varying only the muscle layer thickness.

It is evident in Fig. 51 that when the muscle thickness varies there is a variation in the resonance frequency as well as in the s11 amplitude. However, the frequency remains in a very close range compared to the resonance frequency in Fig. 45.

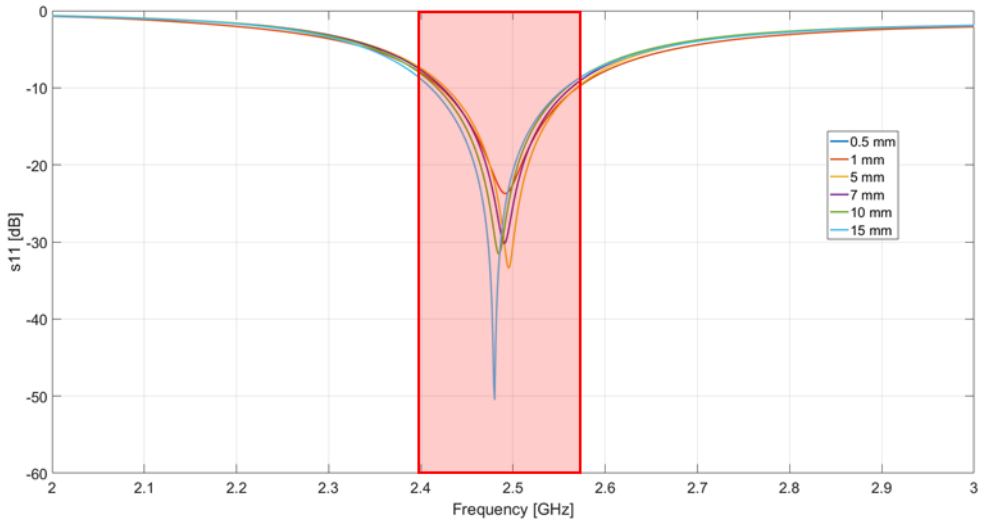

Figure 51 Sensor frequency response varying only the fat layer thickness.

Also in this case, as in the case of the muscle, there is a considerable variation in the amplitude (the 0.5 mm and 1 mm curves are superimposed).

The difference is that the sensor seems more robust to the variation in thickness as far as frequency is concerned, in fact, it varies in an even smaller range (2.48-2.495 GHz) than in the previous case (2.447-2.519 GHz) reported in Fig. 50.

This trend is reported in Fig. 52.

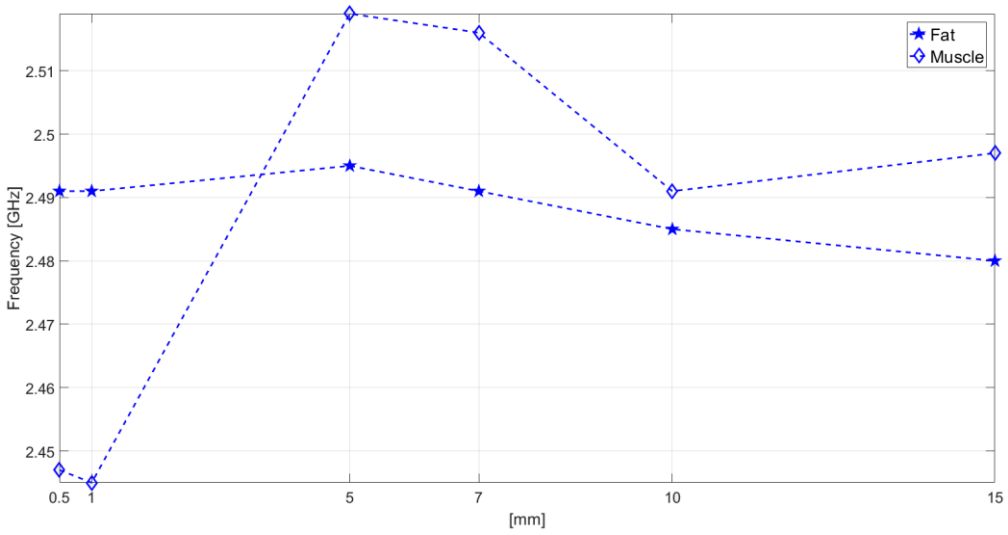

Figure 52 Comparison between the two frequency trends.

This difference depends on the fact that the dielectric constant of the fat layer is much smaller than that of the muscle (see Table 12).

6.9 Bending Effects on the Textile Antenna

After the previous study on the behaviour of the antenna by varying the thickness of the MUT, another important aspect to consider is the bending, in fact the antenna is integrate on the clothing and is in contact with human arm, and it folds following the circumference of the arm [59].
In this analysis two different circumferences are taken into consideration on which to fold the wearable antenna. The two circumferences are those relative to the arm of a male subject and a female subject.
The values of circumferences considered are reported in the Table 14.

Table 14: Medium arm circumference of three different subjects.

Subject	**Radius [cm] (Medium Value)**
Male	5
Female	4.40

In order to simulate the desired bending effect, the textile sensor is folded around a cylinder with variable radius. In Fig. 53, the sensor bending for the different situations is illustrated.

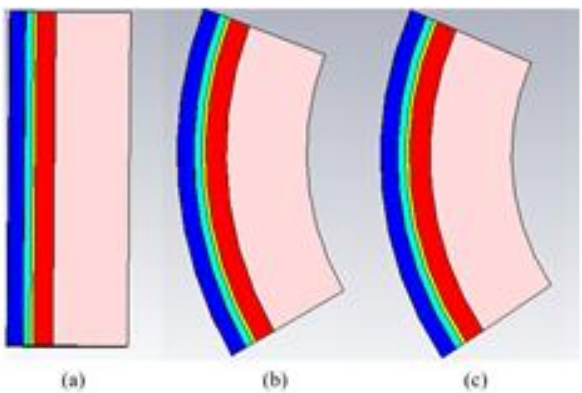

Figure 53(a) Flat conditions wearable sensor. (b) Sensor bent on the male subject arm. (c) Sensor bent on the female subject arm.

The sensor reflective response is evaluated in the above bending conditions, with the corresponding result reported in Fig. 54.

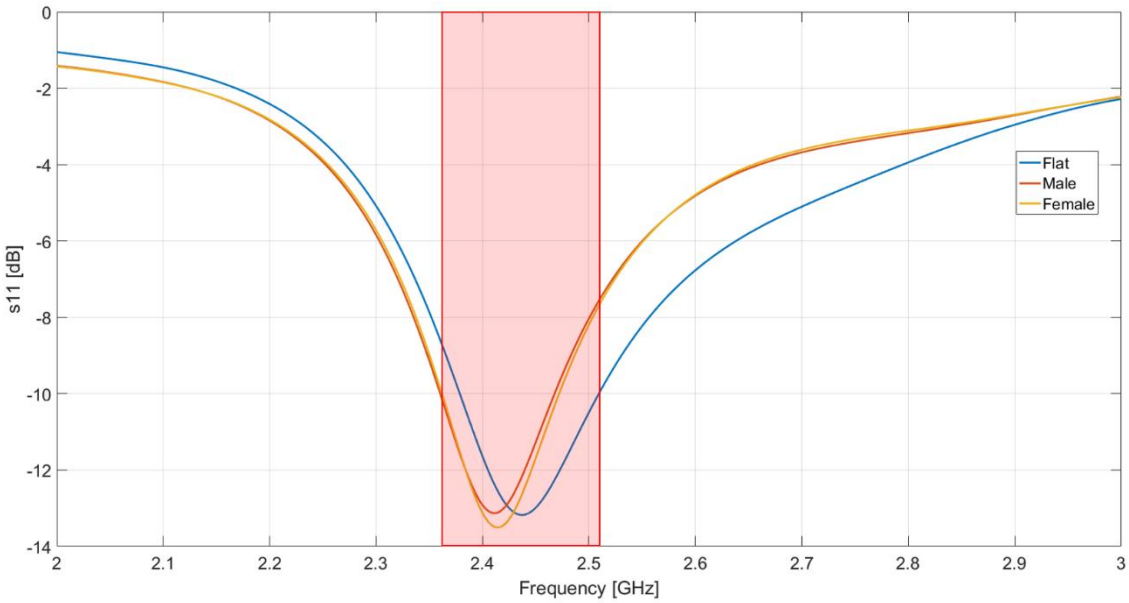

Figure 54 Simulated return loss at different bending conditions.

From the above preliminary analysis, an almost negligible variation in the frequency shift can be observed, when assuming the sensor bending condition.

6.10 Preliminary Specific Absorption Rate (SAR) Analysis

Wearable antennas operate in close proximity of human body, which has a high dielectric constant and conductivity. This antenna works with the radiating element facing the human arm, so the radiation gets penetrated and absorbed in body tissues. The absorption of power per unit mass of human body is evaluated by a term known as the Specific Absorption Rate (SAR), this parameter is a measure of electromagnetic wave penetration in human

body tissues. SAR is a number that measures the speed at which energy is absorbed by the human body when it is exposed to electromagnetic fields with a carrier frequency between 100 kHz and 10 GHz. It is used in different fields, in mobile telephony the SAR establishes the energy absorbed by a particular mass of human tissue within a certain period of time, the SAR is calculated in units of power per mass (W/kg).

The formula is in (27):

$$SAR = \frac{\sigma|E|^2}{\rho} \left[\frac{W}{Kg}\right] \quad (27)$$

where, σ, is the conductivity of the tissue (S/m), ρ, is the mass density of tissue (Kg/m3) and E, is the root mean square of electric field strength (V/m). SAR can also be calculated as rate of temperature rise at a given point, used in some basic research [60].

The evaluated SAR values depend on several parameters: operating frequency, intensity of the field, polarization of the field, source-object configuration (whether the object is in the near or far radiation field), and the characteristics of the exposed body and ground and reflect effects.

In the range between 100 kHz to 10 GHz, restrictions on the SAR are provided in order to prevent entire body heat stress and excessive local tissue heating. Two different exposures have been defined, occupational and general public exposure. The occupational exposure refers to population groups (adults) who are aware of the EM exposures and potential risks and trained to take adequate precautions. By contrast, the general public comprises all the other groups of people of all ages and different health statuses. In many cases, the wider public is not aware of their exposure to the EM radiation and it is not expected that they will take precautions to

minimize or avoid the exposure. Therefore, stricter regulations are required for public as compared to occupational exposure

In order to evaluate the real risk for the human body, some numerical simulations are conducted to measure the SAR levels.

The SAR analysis is carried out using CST Microwave Studio and the standard safe levels are shown below:

- **FCC** [61]**:**
- Body, trunk, head: 1g-SAR with limit 1.6 W/Kg
- Limbs: 10g-SAR with limit 4 W/Kg
- **CE** [62]**:**
- Body, trunk, head: 10g-SAR with limit 2 W/Kg
- Limbs: 10g-SAR with limit 4 W/Kg

Since the sensor must work on the human arm, the safe limit considered is 4 W/Kg for any 10 gram of tissue.

The characteristics considered for the biological superstrate are reported in the Table 15.

Table 15: Characteristics considered for the biological superstrate.

Medium	**Thickness [mm]**	**ε_r**	**tanδ**	**σ [S/m]**	***Density* [kg/m^3]**
Dry Skin	0.015	38.06	0.2835	1.5	1000
Wet Skin	0.985	42.92	0.2727	1.62	1000
Fat	0.5	10.84	0.1808	0.27	850
Blood	2.5	58.53	0.1743	1.41	1060
Muscle	3	52.34	0.1893	1.37	1050

The input power considered on the CAD software is equal to 0.5 W.

In the next figure, is reported the first SAR value considering the wearable textile sensor proposed above.

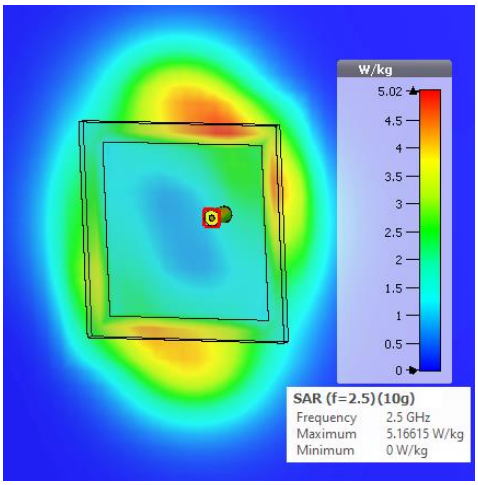

Figure 55 SAR analysis for the first sensor configuration (Fig. 46).

It is evident that with this geometry the SAR value exceeds the permitted safety value, in fact the result is 5.16 W/Kg.

The problem in this application is the medium under test, in fact the SAR is directly proportional to body conductivity and inversely proportional to body permittivity [63].

Human body tissue with higher water content is more susceptible to absorbing radiation, moreover, the body tissue is greater in conductivity which increases SAR values.

There are some different techniques to reduce the SAR, for example use metamaterial to restricts the propagation of surface waves within a specific frequency band and therefore reduce the level of unwanted radiations towards the human body [64], or another technique is to modify the substrate.

In this work, not being able to change the substrate material, its thickness has been changed.

For the first test, its thickness has been increased to 4 mm. After this change, the SAR has been analyzed again, and in the Fig. 56, is reported the result.

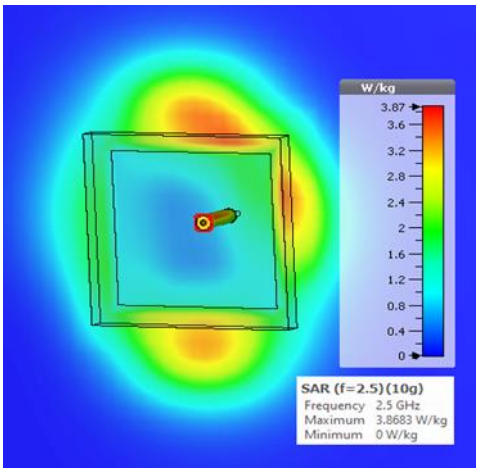

Figure 56 SAR analysis for the sensor configuration with 4 mm substrate thickness.

In this case, the SAR value suffered a sharp decrease, in fact, now the value is 3.86 W/Kg, and is perfectly within the safe limits for humans.
Other simulations have been carried out by varying the substrate thickness and the results are listed in the Table 16.

Table 16: SAR values at different substrate thickness.

Thickness [mm]	**SAR [W/Kg]**
1.5	5.81
2	5.16
4	3.86
5	3.58

An increase in thickness causes a decrease in SAR values, so it is possible to vary the SAR level only varying the substrate thickness, without changing the material [65].

7 ANTENNA PROTOTYPE

This section describes the steps performed during the fabrication process of a wearable textile antenna built using denim and PCPTF and the following measurements made on the realized prototype.

As seen above, the antenna was designed and simulated with the commercially available 3D EM full wave software CST Studio Software [57].

Once obtained the optimal performances, the dimensions of the antenna have been extracted and used for tailoring the fine copper conductive sheet and the denim.

CST model of the wearable sensor and the 2D sketches with all the dimensions are already reported in Fig. 44, in Chapter 6.6.

7.1 Realization of the First Wearable Biosensor Prototype

In order to respect the project dimensions, paper masks have been made on AutoCad [66] then printed so that they could be used in the cutting of materials and above all in the fed position.

Once the fabrics of the correct size have been cut, it is necessary to join ground plane, substrate and patch together. The PCPTF used has the particularity of being adhesive, so it was enough to glue the two conductive layers (ground plane and radiator patch) with the substrate (denim) in the middle.

The final prototype realized is reported in Fig. 57.

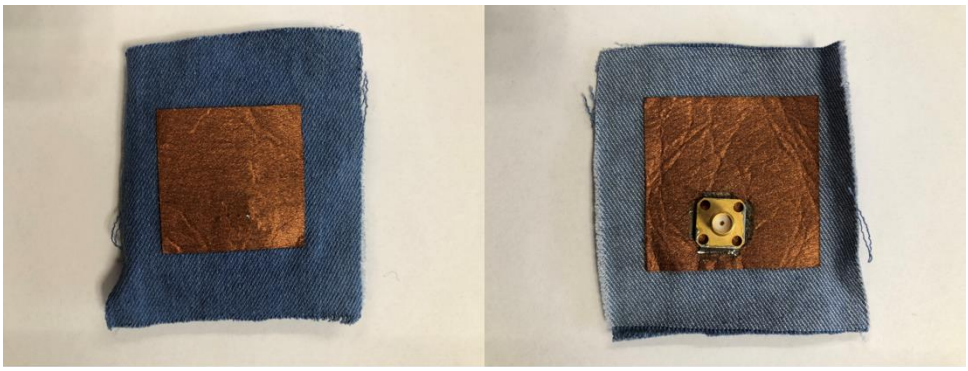

(a) (b)

Figure 57 (a) Front textile wearable sensor. (b) Back textile wearable sensor.

The wearable sensor has a final size of about 4cm x 4cm, so resulting to be very small and easily wearable and integrable with daily clothing, Fig. 58.

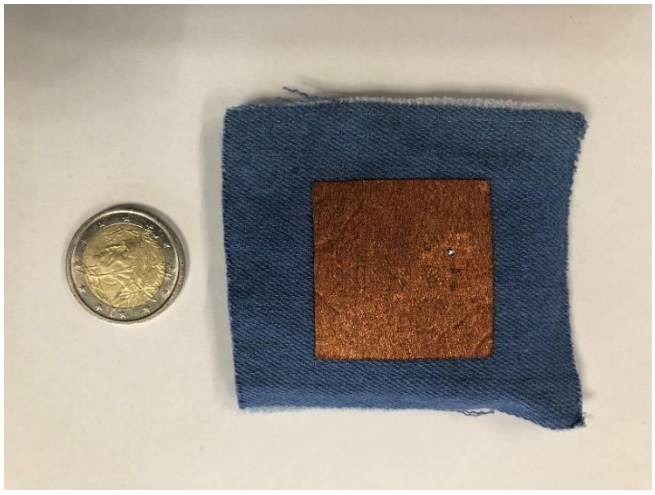

Figure 58 Final sensor dimension compared with the coin size.

Although the realization may seem simple, it's actually not, and the main reasons are different.

A difficulty is to cut out the fabrics as precisely as possible even if this phase is facilitated by the use of paper masks, however, the materials used are rather delicate and therefore subject to imperfections. Moreover, even perfectly positioning the fed is not trivial in fact this will have to cross three layers of different fabrics without bending or moving. The coaxial connector used is the **R125.403.000,** and the dimensions are reported in the Fig. 59, [67].

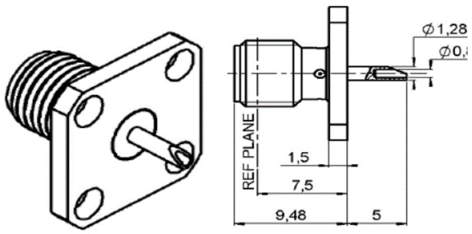

Figure 59 Coaxial connector dimensions.

Also the soldering process between pins and patch could cause problems, in fact at the high temperatures of the welder there is the risk of burning the textiles irreparably compromising their features.
In the following paragraph, will be presented and discussed the experimental validations on the realized biosensor.

7.2 Experimental Validations

Preliminary experimental validations of the realized prototype are performed by measuring its return loss (free-space condition).
The experimental validations are conducted in the µWave Laboratory at the University of Calabria.
The first step was to connect the realized biosensor to the Vector Network Analyzer present in the laboratory, Fig. 60.

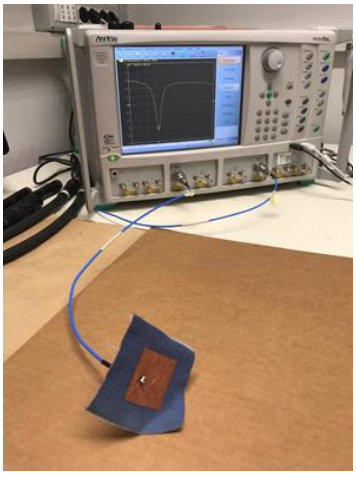

Figure 60 Realized wearable sensor connected to the VNA.

First of all, it has been experimentally validated in the air, Fig. 61.

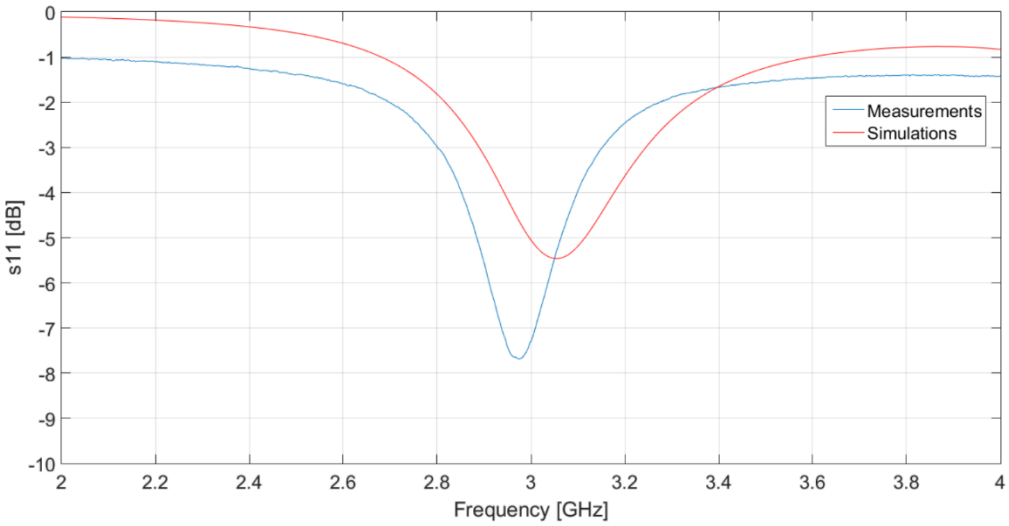

Figure 61 Comparison between the simulation and the measurement in the air.

Then this first measurement, has been performed a measurement with the sensor in contact with the human arm, Fig. 62 and Fig. 63.

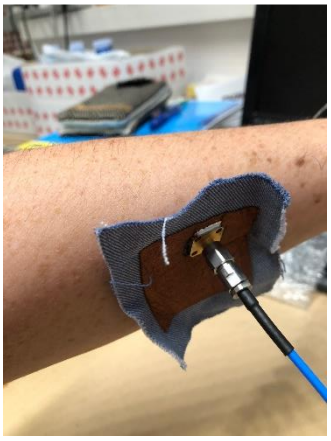

Figure 62 Biosensor in contact with the human arm.

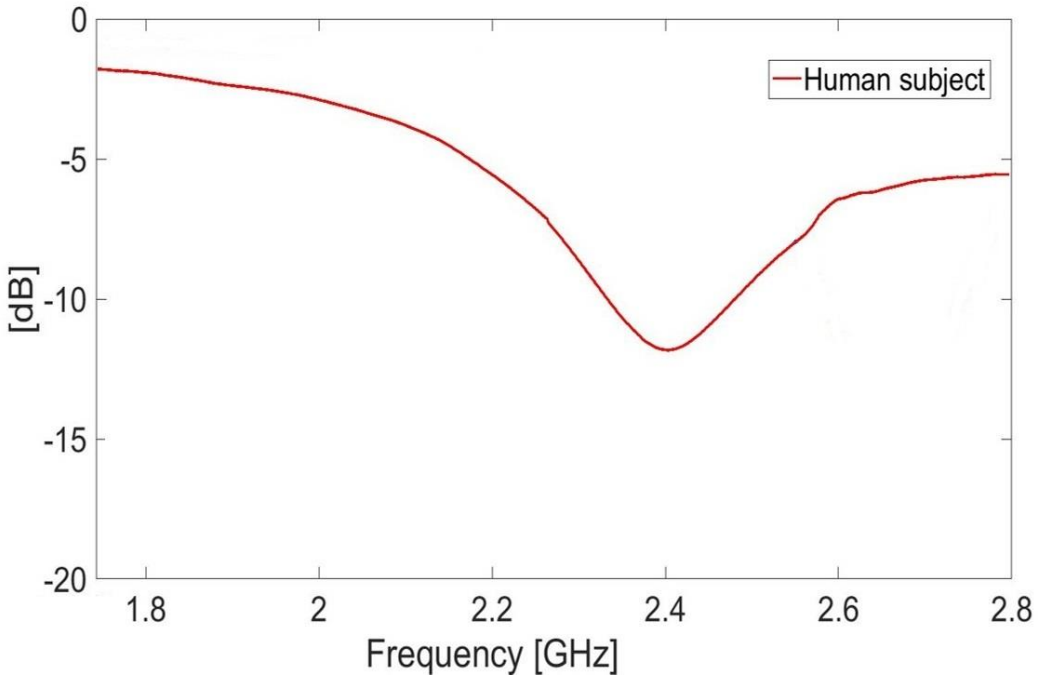

Figure 63 Measurement with the biosensor in contact with human arm.

As expected, a higher resonance frequency is observed when operating in free-space conditions (Fig. 61). A very important result is that, when operating in contact with the human subject, a proper resonant frequency around 2.4 GHz is achieved, which is very close to that obtained in the simulation step when considering a biological superstrate.

8 CONCLUSIONS

Wearable applications and, thus, wearable antennas are becoming an unavoidable part of nowadays wireless communication. Various activities can be accomplished and many of them can be significantly accelerated with the help of wearable applications. For instance, in modern health care, data collected from different sensors (e.g. blood pressure, temperature, etc.) worn by a patient can be transferred to peripheral units (smart phones, tablet) and sent to a hospital or a medical doctor, who can in turn provide feed-back within a couple of minutes.

Many wearable antennas have been reported in the literature, covering different applications and various frequency bands. Nevertheless, there is still no clear overview or guideline on how to tackle the design of wearable antenna for a particular application.

The aim of this thesis was to provide an appropriate wearable antenna design suitable for health applications, more specifically for non-invasive monitoring of blood-glucose concentration inside the commercially used ISM-band.

In this context and specified project requirements, have been defined two main challenges addressed in this thesis: the first was to develop an improved version of the classic Cole-Cole model, the second to use fabrics for both the substrate and the conductive part of the sensor so as to be easily integrated with the clothes.

In Chapter 4 it was shown, in fact, that when the irradiation medium is the biological tissue it is fundamental to characterize the medium under test as accurately as possible.

For this reason, the enhanced version of the Cole-Cole model allows a more precise electromagnetic characterization of the blood layer with different

glucose concentrations, both for the real part of the complex permittivity and the imaginary part.

The importance of the imaginary part, which allows the calculation of the tangent loss factor, as well as already demonstrated in the literature [27], has been further verified, in this thesis, with the comparisons made with the other dielectric models already present in the literature.

In parallel with the elaboration of the enhanced dielectric model, has been analyzed the potential antenna candidates that would respond to the defined requirements, in fact, in the Chapters 6 and 7, has been presented a wearable textile antenna for the monitoring of BGC.

The detailed antenna design has been reported and some numerical and experimental validations have been conducted in order to demonstrate the effectiveness of the proposed approach, also in terms of SAR values.

Moreover, a two-variable function has also been developed which, starting from the return loss measurements, can reconstruct the BGC value in mg/dl.

In this thesis, several aspects related to wearable antennas were addressed. However, there are still open issues and improvements that should be investigated. As a constantly growing field, wearable antennas will remain in the scope of the research for some time. Regardless of the type of application they are intended for, some requirements will remain present: size reduction, improvement of the wearability aspects, improvement of the radiation characteristics, and in-depth measures on biological phantoms.

9 REFERENCES

[1] "WHO | Diabetes," *WHO*, 2013.

[2] "Executive Summary: Standards of Medical Care in Diabetes-2010," 2010.

[3] T. Koschinsky, K. Jungheim, and L. Heinemann, "Glucose sensors and the alternate site testing-like phenomenon: relationship between rapid blood glucose changes and glucose sensor signals.," *Diabetes Technol. Ther.*, vol. 5, no. 5, pp. 829–42, 2003.

[4] T. Koschinsky and L. Heinemann, "Sensors for glucose monitoring: technical and clinical aspects.," *Diabetes. Metab. Res. Rev.*, vol. 17, no. 2, pp. 113–23.

[5] B. Aussedat, M. Dupire-Angel, R. Gifford, J. C. Klein, G. S. Wilson, and G. Reach, "Interstitial glucose concentration and glycemia: Implications for continuous subcutaneous glucose monitoring," *Am. J. Physiol. - Endocrinol. Metab.*, vol. 278, no. 4 41-4, Apr. 2000.

[6] J. K. Nielsen *et al.*, "Continuous glucose monitoring in interstitial subcutaneous adipose tissue and skeletal muscle reflects excursions in cerebral cortex.," *Diabetes*, vol. 54, no. 6, pp. 1635–9, Jun. 2005.

[7] A. Tura, A. Maran, and G. Pacini, "Non-invasive glucose monitoring: Assessment of technologies and devices according to quantitative criteria," *Diabetes Research and Clinical Practice*. 2007.

[8] D. Guo, D. Zhang, and N. Li, "Monitor blood glucose levels via breath analysis system and sparse representation approach," in *Proceedings of IEEE Sensors*, 2010.

[9] O. S. Khalil, "Non-invasive glucose measurement technologies: an update from 1999 to the dawn of the new millennium.," *Diabetes Technol. Ther.*, vol. 6, no. 5, pp. 660–97, Oct. 2004.

[10] S. Liakat, K. A. Bors, L. Xu, C. M. Woods, J. Doyle, and C. F. Gmachl, "Noninvasive in vivo glucose sensing on human subjects using mid-infrared light.," *Biomed. Opt. Express*, vol. 5, no. 7, pp. 2397–404, Jul. 2014.

[11] K. V Larin, M. S. Eledrisi, M. Motamedi, and R. O. Esenaliev, "Noninvasive blood glucose monitoring with optical coherence tomography: a pilot study in human subjects.," *Diabetes Care*, vol. 25, no. 12, pp. 2263–7, Dec. 2002.

[12] S. J. Yeh, C. F. Hanna, and O. S. Khalil, "Monitoring blood glucose changes in cutaneous tissue by temperature-modulated localized reflectance measurements," *Clin. Chem.*, 2003.

[13] E. B. Hanlon *et al.*, "Prospects for in vivo Raman spectroscopy," *Physics in Medicine and Biology*. 2000.

[14] R. W. Waynant and V. M. Chenault, "Overview of Non-Invasive Optical Glucose Monitoring Techniques- Overview of Non-Invasive Fluid Glucose Measurement Using Optical Techniques to Maintain Glucose Control in Diabetes Mellitus."

[15] Y. Shen *et al.*, "Measurement of the optical absorption coefficient of a liquid by use of a time-resolved photoacoustic technique," 2000.

[16] A. Domschke *et al.*, “Holographic sensors in contact lenses for minimally-invasive glucose measurements,” 2006.

[17] C. E. Ferrante do Amaral and B. Wolf, “Current development in non-invasive glucose monitoring,” *Medical Engineering and Physics*. 2008.

[18] S. K. Vashist, “Continuous Glucose Monitoring Systems: A Review.,” *Diagnostics (Basel, Switzerland)*, vol. 3, no. 4, pp. 385–412, Oct. 2013.

[19] T. Yilmaz, R. Foster, and Y. Hao, “Broadband tissue mimicking phantoms and a patch resonator for evaluating noninvasive monitoring of blood glucose levels,” *IEEE Trans. Antennas Propag.*, 2014.

[20] M. Hofmann, G. Fischer, R. Weigel, and D. Kissinger, “Microwave-based noninvasive concentration measurements for biomedical applications,” *IEEE Trans. Microw. Theory Tech.*, 2013.

[21] B. J. Klauenberg and D. Miklavčič, *Radio Frequency Radiation Dosimetry and Its Relationship to the Biological Effects of Electromagnetic Fields*. 2000.

[22] “Polar molecules. By P. Debye, Ph.D., Pp. 172. New York: Chemical Catalog Co., Inc., 1929.,” *J. Soc. Chem. Ind.*, vol. 48, no. 43, pp. 1036–1037, Oct. 1929.

[23] R. H. C. K. H. Cole, “Dispersion and Absorption in Dielectrics 1.,” vol. I, no. 1913, 1941.

[24] S. Gabriel, R. W. Lau, and C. Gabriel, “The dielectric properties of biological tissues : III . Parametric models for the dielectric spectrum of tissues,” vol. 41, pp. 2271–2293, 1996.

[25] T. Karacolak, E. C. Moreland, and E. Topsakal, “Cole-cole model for glucose-dependent dielectric properties of blood plasma for continuous glucose monitoring,” *Microw. Opt. Technol. Lett.*, vol. 55, no. 5, pp. 1160–1164, May 2013.

[26] J. Venkataraman and B. Freer, “Feasibility of non-invasive blood glucose monitoring: In-vitro measurements and phantom models,” *IEEE Antennas Propag. Soc. AP-S Int. Symp.*, pp. 603–606, 2011.

[27] S. Costanzo, “Loss tangent effect on the accurate design of microwave sensors for blood glucose monitoring,” in *2017 11th European Conference on Antennas and Propagation, EUCAP 2017*, 2017, pp. 661–663.

[28] S. Costanzo, V. Cioffi, and A. Raffo, “Analytical model for microwave sensors behavior into biological medium,” *2017 IEEE Int. Conf. Microwaves, Antennas, Commun. Electron. Syst. COMCAS 2017*, vol. 2017-Novem, pp. 1–4, 2017.

[29] V. Turgul and I. Kale, “On the accuracy of complex permittivity model of glucose/water solutions for non-invasive microwave blood glucose sensing,” *2015 E-Health Bioeng. Conf. EHB 2015*, 2016.

[30] S. Costanzo, V. Cioffi, and A. Raffo, “Complex permittivity effect on the performances of non-invasive microwave blood glucose sensing: Enhanced model and preliminary results,” in *Advances in Intelligent Systems and Computing*, 2018, vol. 746, pp. 1505–1511.

[31] S. Costanzo, “Non-invasive microwave sensors for biomedical applications: New design perspectives,” *Radioengineering*, vol. 26, no. 2, pp. 406–410, Jun. 2017.

[32] D. M. Nathan *et al.*, “Intensive diabetes treatment and cardiovascular disease in patients with type 1 diabetes,” *N. Engl. J. Med.*, vol. 353, no. 25, pp. 2643–2653, Dec. 2005.

[33] D. G. Rogers, “The effect of intensive treatment of diabetes on the development and progression of long-term complications in insulin-dependent diabetes mellitus,” *Clinical Pediatrics*, vol. 33, no. 6. p. 378, 1994.

[34] American Diabetes Association, “Standards of medical care in diabetes--2006.,” *Diabetes Care*, vol. 29 Suppl 1, pp. S4-42, Jan. 2006.

[35] W. L. Clarke, “The Original Clarke Error Grid Analysis (EGA),” in *Diabetes Technology and Therapeutics*, 2005, vol. 7, no. 5, pp. 776–779.

[36] D. Psychoudakis, G. Lee, C. Chen, and J. L. Volakis, “Military UHF Body-Worn Antennas for Armored Vests,” *Proc. Fourth Eur. Conf. Antennas Propag.*, pp. 1–4.

[37] C. Hertleer, H. Rogier, L. Vallozzi, and L. Van Langenhove, “A textile antenna for off-body communication integrated into protective clothing for firefighters,” *IEEE Trans. Antennas Propag.*, vol. 57, no. 4 PART. 1, pp. 919–925, 2009.

[38] A. A. Serra, P. Nepa, and G. Manara, “A wearable multi antenna system on a life jacket for Cospas Sarsat rescue applications,” in *IEEE Antennas and Propagation Society, AP-S International Symposium (Digest)*, 2011, pp. 1319–1322.

[39] D. Psychoudakis and J. L. Volakis, “Conformal asymmetric meandered flare (AMF) antenna for body-worn applications,” *IEEE Antennas Wirel. Propag. Lett.*, vol. 8, pp. 931–934, 2009.

[40] L. Vallozzi, W. Vandendriessche, H. Rogier, C. Hertleer, and M. L. Scarpello, “Wearable textile GPS antenna for integration in protective garments,” *EuCAP 2010 - 4th Eur. Conf. Antennas Propag.*, pp. 1–4, 2010.

[41] A. Dierck, H. Rogier, and F. Declercq, “A wearable active antenna for global positioning system and satellite phone,” *IEEE Trans. Antennas Propag.*, vol. 61, no. 2, pp. 532–538, 2013.

[42] X. L. Chen, N. Kuster, Y. C. Tan, and N. Chavannes, “Body effects on the GPS antenna of a wearable tracking device,” in *Proceedings of 6th European Conference on Antennas and Propagation, EuCAP 2012*, 2012, pp. 3313–3316.

[43] J.-F. Zurcher, O. Staub, and A. K. Skrivervik, “SMILA: A compact and efficient antenna for mobile communications,” *Microw. Opt. Technol. Lett.*, vol. 27, no. 3, pp. 155–157, Nov. 2000.

[44] M. Lapinski, M. Feldmeier, and J. A. Paradiso, “Wearable wireless sensing for sports and ubiquitous interactivity,” in *Proceedings of IEEE Sensors*, 2011, pp. 1425–1428.

[45] D. Gaetano, P. McEvoy, M. J. Ammann, J. E. Browne, L. Keating, and F. Horgan, “Footwear antennas for body area telemetry,” *IEEE Trans. Antennas Propag.*, vol. 61, no. 10, pp. 4908–4916, 2013.

[46] D. Gaetano, P. McEvoy, M. J. Ammann, C. Brannigan, L. Keating, and F. Horgan, “Footwear and wrist communication links using 2.4 GHz and UWB antennas,”

Electron. , vol. 3, no. 2, pp. 339–350, Jun. 2014.

[47] "Zegna Sport Bluetooth iJacket incorporates smart fabric." [Online]. Available: https://newatlas.com/go/7856/.

[48] "Verb for Shoe - very intelligent shoes!" [Online]. Available: https://newatlas.com/go/3565/.

[49] D. P. Tobón, T. H. Falk, and M. Maier, "Context awareness in WBANs: A survey on medical and non-medical applications," *IEEE Wireless Communications*, vol. 20, no. 4. pp. 30–37, 2013.

[50] Z. Popovic, P. Momenroodaki, and R. Scheeler, "Toward wearable wireless thermometers for internal body temperature measurements," *IEEE Commun. Mag.*, vol. 52, no. 10, pp. 118–125, Oct. 2014.

[51] F. Axisa, P. M. Schmitt, C. Gehin, G. Delhomme, E. McAdams, and A. Dittmar, "Flexible technologies and smart clothing for citizen medicine, home healthcare, and disease prevention.," *IEEE Trans. Inf. Technol. Biomed.*, vol. 9, no. 3, pp. 325–36, Sep. 2005.

[52] K. B. Yu, S. G. Ogourtsov, V. G. Belenky, A. B. Maslenikov, and A. S. Omar, "Accurate microwave resonant method for complex permittivity measurements of liquids," *IEEE Trans. Microw. Theory Tech.*, vol. 48, pp. 2159–2164, 2000.

[53] R. Salvado, C. Loss, Gon, and P. Pinho, "Textile materials for the design of wearable antennas: A survey," *Sensors (Switzerland)*, vol. 12, no. 11. pp. 15841–15857, Nov-2012.

[54] J. C. G. Matthews and G. A. Pettitt, "Development of flexible, wearable antennas," 2009.

[55] "About ITU." [Online]. Available: https://www.itu.int/en/about/Pages/default.aspx.

[56] V. Cioffi and S. Costanzo, "Wearable approach for contactless blood-glucose monitoring by textile antenna sensor," *Adv. Intell. Syst. Comput.*, vol. 932, pp. 287–291, 2019.

[57] "CST Studio Suite 3D EM simulation and analysis software." [Online]. Available: https://www.3ds.com/products-services/simulia/products/cst-studio-suite/.

[58] V. Cioffi, A. Raffo, and S. Costanzo, "Preliminary Validations of Textile Wearable Microwave Sensor for Biomedical Applications," *13th Eur. Conf. Antennas Propagation, EuCAP 2019*, no. EuCAP, pp. 1–2, 2019.

[59] S. Costanzo and V. Cioffi, "Full Analysis of Wearable Textile Sensor for Biomedical Applications : Preliminary Validations Towards a Pre-Clinical Assessment," *14th Eur. Conf. Antennas Propagation, EuCAP 2020*, 2020.

[60] M. T. Islam, H. Z. Abidin, M. R. I. Faruque, and N. Misran, "Analysis of materials effects on radio frequency electromagnetic fields in human head," *Prog. Electromagn. Res.*, vol. 128, pp. 121–136, 2012.

[61] "https://www.fcc.gov/search/#q=specific%20absorp." .

[62] "Official Journal of the European Communities, L 199/59, 2 July 1999." [Online].

Available: https://eur-lex.europa.eu/LexUriServ/LexUriServ.do?uri=OJ:L:1999:199:0059:0070:EN:PDF.

[63] N. A. Husni, M. T. Islam, M. R. I. Faruque, N. Misran, and M. T. Islam, “Effects of Electromagnetic Absorption Towards Human Head Due to Vriation of its Dielectric Properties at 900, 1800 and 1900 MHz with Different Antenna Substrates,” 2013.

[64] U. Ali *et al.*, “Design and SAR analysis of wearable antenna on various parts of human body, using conventional and artificial ground planes,” *J. Electr. Eng. Technol.*, vol. 12, no. 1, pp. 317–328, 2017.

[65] S. Costanzo and V. Cioffi, “Preliminary SAR Analysis of Textile Antenna Sensor for Non-invasive Blood-Glucose Monitoring Standard Coaxial Probe Fed Patch Antenna on Textile Substrate,” pp. 1–6.

[66] “AutoCAD for Mac e Windows | Software CAD | Autodesk.” [Online]. Available: https://www.autodesk.it/products/autocad/overview.

[67] “R125403000 Radiall | Mouser Europe.” [Online]. Available: https://eu.mouser.com/ProductDetail/Radiall/R125403000?qs=sGAEpiMZZMuLQf%252BEuFsOrsLGtpGYO%2FccfJFnYqMKuAk%3D.

10 PUBLICATIONS

International Conferences:

- S. Costanzo, V. Cioffi, A. Raffo, *"Complex Permittivity Effect on the Performances of Non-Invasive Microwave Blood Glucose Sensing: Enhanced Model and Preliminary Results",* WorldCist'18, Napoli, Italia.
- A. Raffo, S. Costanzo, V. Cioffi, "*Quadrature Receiver Benefits in CW Doppler Radar Sensors for Vibrations Detection",* WorldCist'18, Napoli, Italia. **(1st Position in the best conference paper competition)**
- V. Cioffi, "*Enhanced Cole-Cole Dielectric Model for Accurate Blood Glucose Sensing",* XXII RiNEm 2018, Cagliari, Italia.
- A. Raffo, V. Cioffi, S. Costanzo, "*Software-Defined Radar for Vital Sign Monitoring",* XXII RiNEm 2018, Cagliari, Italia. **(Premio CNIT).**
- V. Cioffi, A. Raffo, and S. Costanzo, "*Preliminary validations of textile wearable microwave sensor for biomedical applications*", 13th European Conference on Antennas and Propagation, EuCAP 2019.
- V. Cioffi, and S. Costanzo, "*Wearable approach for contactless blood-glucose monitoring by textile antenna sensor"*, WorldCIST'19, La Toja Island, Spain (2019).
- S. Costanzo and V. Cioffi, *"Dielectric Models for the Accurate Design of Wearable Diabetes Sensors",* ICECOM 2019, Dubrovnik, Croatia.
- S. Costanzo and V. Cioffi, *"Preliminary SAR Analysis of Textile Antenna Sensor for Non-invasive Blood-Glucose Monitoring",* ICITS'20, Bogotà, Colombia.
- S. Costanzo and V. Cioffi, *"Fully Analysis of Wearable Textile Sensor for Biomedical Applications: Preliminary Validations Towards a Pre-Clinical Assessment",* EUCAP 2020, Copenhagen, Denmark. (in press)

International Journals:

- S. Costanzo and V. Cioffi, *"Microwave Dielectric Models for the Prediction of Blood Glucose Concentration in Smart Medicine: Overview and New Developments",* International Journal of Antennas and Propagation – Bioengineering Applications of Electromagnetic Wave Propagation, Hindawi, 2019. (Under Review)